Ana Filipa Santos Seiça

Molecule - colloidal particle interactions: Raman spectroscopic studies

Tese de Mestrado em Bioquímica

Julho de 2016

· U C ·

UNIVERSIDADE DE COIMBRA

FCTUC FACULDADE DE CIÊNCIAS E TECNOLOGIA
UNIVERSIDADE DE COIMBRA

Molecule – colloidal particle interactions: Raman spectroscopic studies

Dissertação apresentada ao Departamento de Ciências da Vida da Universidade de Coimbra para a obtenção do Grau de Mestre em Bioquímica

Orientador – Professor Doutor José Joaquim Cristino Teixeira Dias
Categoria – Professor Catedrático Jubilado
Afiliação – Departamento de Química Física Molecular da Universidade de Coimbra

Orientador – Professor Doutor Juan Carlos Otero Fernández de Molina
Categoria – Professor Catedrático
Afiliação – Departamento de Química Física da Universidade de Málaga

Ana Filipa Santos Seiça

2016

Dedico esta tese à Minha Família,

sem eles nunca teria atingido os objectivos

propostos para este percurso académico.

Ajudaram-me a crescer e a acreditar em mim.

São o pilar, a minha segurança, para avançar todos os dias e conquistar o "Mundo".

“I cannot move forward without my wins and my losses
This is what makes me stronger
becoming resistant
When life is hard it challenges you
if things were easy life
would amount to nothing, it wouldn't be worth living
I will fight for the things I love
and whatever doesn't matter to me will fade into
the darkness as quick as it appeared
I leave behind a memory
which will forever be treasured by others who finds it
To be content with the pursuit is the ultimate goal
I would like to be happy with where I am in life
I want to enjoy it
I live, I learn, I love
and will love being free until the end.”

Marcquiese Burrell,1987

Acknowledgements

O meu agradecimento especial a todos que contribuíram para a realização deste estudo sendo imperativo a sua referenciação:

Ao meu Orientador, o Sr. Professor Doutor José Joaquim Cristino Teixeira Dias por aceitar tal compromisso, pela inteira disponibilidade sempre demonstrada, paciência, humanidade, simpatia, partilha do seu saber, objectividade e imprescindíveis sugestões durante toda a criação, execução do estudo e realização do artigo científico;

Ao meu Orientador Sr. Professor Doutor Juan Carlos Otero Fernández de Molina pelo acolhimento na Universidade de Málaga, disponibilidade e partilha de conhecimentos;

À Srª. Professora Maria Paula Matos Marques Catarro da Universidade de Coimbra, pela sua disponibilidade durante o curso e pela realização de indiligências e comunicações necessárias com a Universidade de Málaga. O apoio e a sua objectividade bem como a permissão para participar na sua Equipa de Colaboradores, contribuíram para o meu crescimento pessoal e profissional;

Ao Sr. Professor Luís Alberto Batista de Carvalho da Universidade de Coimbra, pelo apoio na concretização do artigo científico, motivação e disponibilidade na recolha dos espectros;

À Srª. Professora Doutora Isabel López Tocón pelo acolhimento realizado na Universidade de Málaga, partilha de conhecimentos e acompanhamento na área experimental;

À Srª. Professora Doutora María Rosa López Ramírez da Universidade de Málaga, pelo acompanhamento na análise dos espectros, partilha de conhecimentos e incentivo;

À Cristina Ruano Frías, Investigadora na Universidade de Málaga, pela disponibilidade, apoio, atenção e acompanhamento na realização dos espectros;

Ao Departamento de Química Física Molecular da Universidade de Coimbra e Departamento de Química Física da Universidade de Málaga pela cedência do espaço, reagentes químicos e aparelhos instrumentais sem custos adicionais;

À minha família pela força, apoio, carinho, afecto, atenção, paciência, preocupação e motivação, em suma, estarem sempre presentes o que, me permite “voar”;

Aos meus amigos que de alguma forma, motivaram e incentivaram à realização do estudo.

Abbreviations

Ag_{np} – Silver Nanoparticles

CDs – Cyclodextrins

D_2O – Deuterated Water

EF - Enhancement Factor

IR - Infrared

mCDs – Methylate Cyclodextrins

NaDec – Sodium Decanoate

RR - Resonance Raman

***t*-CIA** – *trans*-Cinnamic Acid

TRIMEB – heptakis(2,3,6-tri-O-metil)-cyclodextrin-β

αCD – α-cyclodextrin

βCD – β-cyclodextrin

Acronyms

AFM – Atomic Force Microscopy

CMC – Critical Micelle Concentration

CT - Charge Transfer

CM – Chemical Mechanism

EM - Electromagnetic Mechanism

Ɛr – Dielectric Permittivity

FT-IR - Fourier Transform Infrared Spectroscopy

FT-Raman - Fourier Transform Raman Spectroscopy

FWHH - Full Widths at Half Height

***K*a** – Constant Inclusion

LUMO - Lowest Unoccupied Molecular Orbital

NMR – Nuclear Magnetic Resonance

SANS – Small Angle Neutron Scattering

SERS – Surface Enhanced Raman Spectroscopy

UV – Ultra Violet

UV–vis-NIR – Ultra Violet – visible - Near Infrared

ν_m - Molecule Vibrational Frequency

ν_0 – Visible region

Abstract

This thesis aims to analyze the behaviour of natural cyclodextrins and methylate cyclodextrins with colloidal particles - micelles of sodium decanoate and silver nanoparticles using Raman Spectroscopy and Surface Enhanced Raman Spectroscopy. We held the first part in the Molecular Physics Chemistry Department at the University of Coimbra and the second part in the Physics and Chemistry Department at University of Malaga.

In the first part, we deal with sodium decanoate aqueous solutions, above and below the critical micellar concentration, that contain trimethyl-β-cyclodextrin or β-cyclodextrin. A method for calibrating Raman intensities of diluted aqueous solutions, based on the integrated intensity of the OH stretching bands of liquid water as an external intensity standard, is described and used to obtain a difference spectrum that reveals intensity changes mainly due the intermolecular interaction between two solutes. This method was applied to trimethyl-β-cyclodextrin in sodium decanoate aqueous solutions. The difference between the interaction spectra above and below the critical micellar contribution of sodium decanoate, in the CH stretching region between 2700 and 3100 cm^{-1}, shows an intensity increase of the CH stretching bands for trimethyl-β-cyclodextrin above the critical micellar concentration of sodium decanoate, whereas β-cyclodextrin is relatively insensitive to the presence of decanoate ion micelles in aqueous solution. This part of the thesis led to a publication entitled "Raman spectroscopic evidence for the inclusion of decanoate ion in trimethyl-β-cyclodextrin" [Annex 2].

In Part II, we observed the interaction of native and methylate cyclodextrins with *trans*-cinnamic acid and silver colloidal particles using Surface Enhanced Raman Spectroscopy. Native cyclodextrins are adsorbed on the surface of silver colloidal particles via chemisorption through rim hydroxyl groups, stabilizing the colloidal solution during 45 minutes, whereas TRIMEB stabilizes silver nanoparticles during 90 minutes. TRIMEB acts as a better surface stabilizer than βCD, improving the stability of colloidal solution and preventing aggregation.

Finally, native and methylated cyclodextrins exhibit different behaviours in presence of colloidal particles. TRIMEB is adsorbed on the surface of sodium decanoate

micelles , contrasting with βCD which is not adsorbed by these micelles,. In presence of silver nanoparticles natural cyclodextrin is adsrobed on the surface of silver colloidal particles while methylate cyclodextrin is not adsorbed.

Key words: Cyclodextrins, sodium decanoate, micelle, silver nanoparticles, Raman Spectroscopy, Surface Enhanced Raman Spectroscopy.

Resumo

O presente trabalho visa analisar o comportamento das ciclodextrinas naturais e metiladas nas suas interações com partículas coloidais - micelas de decanoato de sódio e nanopartículas de prata e foi realizado no Departamento de Química-Física Molecular da Universidade de Coimbra durante três semestres, se onde utilizou a Espectroscopia de Raman, e no Departamento de Química-Física da Universidade de Málaga (um semestre), onde se recorreu à Espectroscopia de Raman com Intensificação à Superfície.

A primeira parte deste estudo envolveu o estudo de soluções aquosas de decanoato de sódio, acima e abaixo da concentração micelar crítica, contendo trimetil-ciclodextrina-β ou ciclodextrina-β. Um método para calibrar intensidades Raman de soluções aquosas, com base nas bandas de elongação OH da água líquida, como padrão de intensidade externa, é descrito e utilizado para obter um espetro de diferença que revela alterações de intensidade devido a interações intermoleculares entre dois solutos. Este método é aplicado à trimetil-ciclodextrina-β em soluções aquosas de decanoato de sódio. A diferença entre os espectros de interação acima e abaixo da concentração micelar crítica de decanoato de sódio, na região de CH entre 2700 e 3100 cm^{-1}, mostra um aumento de intensidade nas bandas de elongação CH de trimetil-ciclodextrina-β acima da concentração micelar crítica de decanoato de sódio, ao passo que a ciclodextrina-β é relativamente insensível à presença de micelas de decanoato em solução aquosa. Este trabalho originou uma publicação intitulada "Raman spectroscopic evidence for the inclusion of decanoate ion in trimethyl-β-cyclodextrin" [Anexo 2].

Na segunda parte deste estudo, observámos a interação das ciclodextrinas nativas e metiladas com ácido *trans*-cinâmico e as particulas coloidais de prata, por Espectroscopia Raman com Intensificação à Superfície. As ciclodextrinas nativas são adsorvidas quimicamente à superfície de partículas coloidais de prata através dos grupos hidroxilo presentes na cavidade externa da ciclodextrina estabilizando a solução durante 45 minutos, enquanto a TRIMEB estabiliza a solução durante 90 minutos. Relativamente à βCD, a ciclodextrina metilada age como melhor estabilizador das nanopartículas, melhorando a estabilidade da solução coloidal e prevenindo agregação.

Da análise dos dois estudos efectuados, concluímos que as ciclodextrinas naturais e as ciclodextrinas metiladas apresentam comportamentos diferentes na presença de partículas coloidais.

A TRIMEB é absorbida à superfície das micelas de decanoato de sódio, enquanto a βCD não é adsorbida pelas micelas. Na presença de nanopartículas de prata, a ciclodextrina natural é adsorbida à superficie das particulas coloidais de prata, contrastando com a ciclodextrina metilada que não é adsorbida.

Palavras-chave: Ciclodextrina, decanoato de sódio, micela, nanopartículas de prata, Espectroscopia de Raman, Espectroscopia de Raman com Intensificação à Superfície.

INDEX

EXPERIMENTAL SECTION

RESULTS AND DISCUSSION

List of Figures

List of Tables

INTRODUCTION

This thesis aims to analyze the behaviour of natural cyclodextrins (CDs) and methylate cyclodextrins (mCDs), by studying the influence of cyclodextrin methylation (replacement of OH groups by OCH_3 fragments) in interactions with colloidal particles such as micelles of sodium decanoate (NaDec) and silver nanoparticles (Ag_{np}) using Raman Spectroscopy and Surface Enhanced Raman Spectroscopy (SERS). We held the first part in Molecular Physical Chemistry Department at the University of Coimbra and the second part in Physical Chemistry Department at the University of Malaga, Spain (Annex 1).

Cyclodextrins contain a hydrophobic cavity surrounded by a hydrophilic exterior composed of primary and secondary hydroxyl (OH) groups. This cavity can form inclusion complexes with a variety of hydrophobic guest molecules [76]. The relatively weak cyclodextrin - guest interactions will be analyzed by Raman Spectroscopy.

It has been shown by small-angle neutron scattering (SANS) that ammonium decanoate in deuterated water (D_2O) solution originates spherical micelles [12-17], with the occurrence of a critical micellar concentration (CMC) approximately equal to 116 mM. With an increase of temperature, the mobility of decanoate ion chains in the micelles is improved and the methyl groups tend to spend more time near the micelle-water interfaces [3]. Applications of Raman Spectroscopy in amphiphile-water systems have shown that this technique provides information on the structure of the hydrocarbon chain regions [53].

When a cyclodextrin is added to a 200 mM perdeuterated sodium decanoate NaDec(d_{19}) solution in D_2O (CMC = 116 mM), methylate cyclodextrins shows correlation peaks in SANS I(Q) distributions that reflect the degree of methylation, whereas αCD and βCD do not originate any correlation maximum [4], a result which seems to exclude the formation of mixed micelles, at least for this surfactant with the above mentioned concentration [4]. Hence, the study by SANS suggests that methylate cyclodextrins are adsorbed on the surface of the decanoate micelles, giving rise to a balance between molecules in aqueous solution and the molecules adsorbed by micelles (Figure 1). On the other hand, unsubstituted CDs weren't adsorbed by micelles, keeping an inclusion equilibrium in aqueous solution with the decanoate ion [4].

The different behaviours of methylate and natural cyclodextrins with sodium decanoate micelles find some support on the experimental determination of dielectric permittivity (Ɛr) in a interface mica-water, by atomic force microscopy (AFM). In this interface [76] the relative permittivity equals 4 (liquid paraffin has Ɛr = 4.8) and increases to Ɛr = 80 about 100 Å away from the interface within the aqueous solution (Figure 2). In fact, the dipoles of the water molecules in free region of electric double layer are closely aligned, resulting in a much lower dielectric permittivity on the interior of water.

The connection of these results with the different modes of interaction between methylate and non-substituted cyclodextrins with sodium decanoate micelles appears to be understandable: the mCDs are more likely to be adsorbed on the surface of sodium decanoate micelles than the natural CDs, because they experience an environment with a permittivity lower than the water inside so, more energy consistent with the relative permittivity of the own mCDs [78].

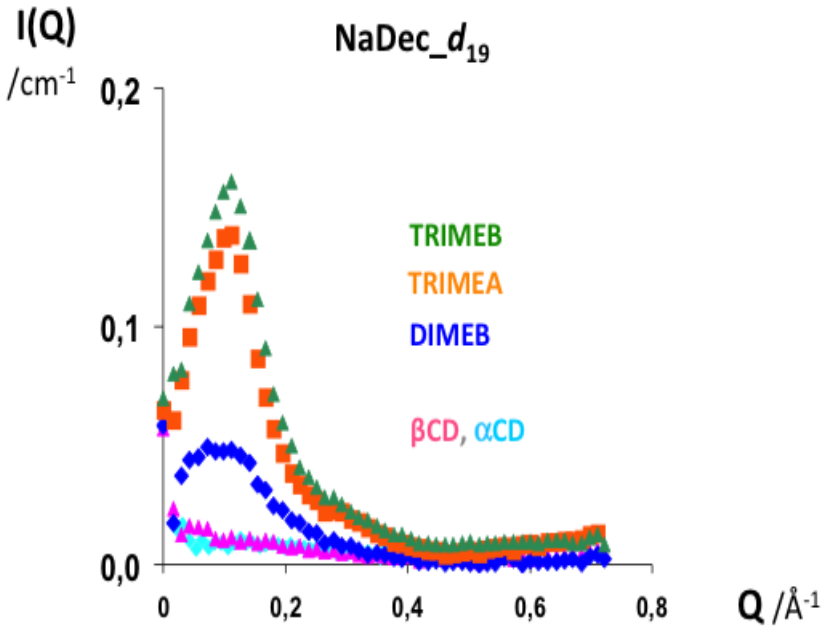

Figure 1 - SANS results for a solution of sodium decanoate perdeuterated 200 mM in D_2O at room temperature in the presence of a cyclodextrin ($[CD]_0$=30 mM) [4].

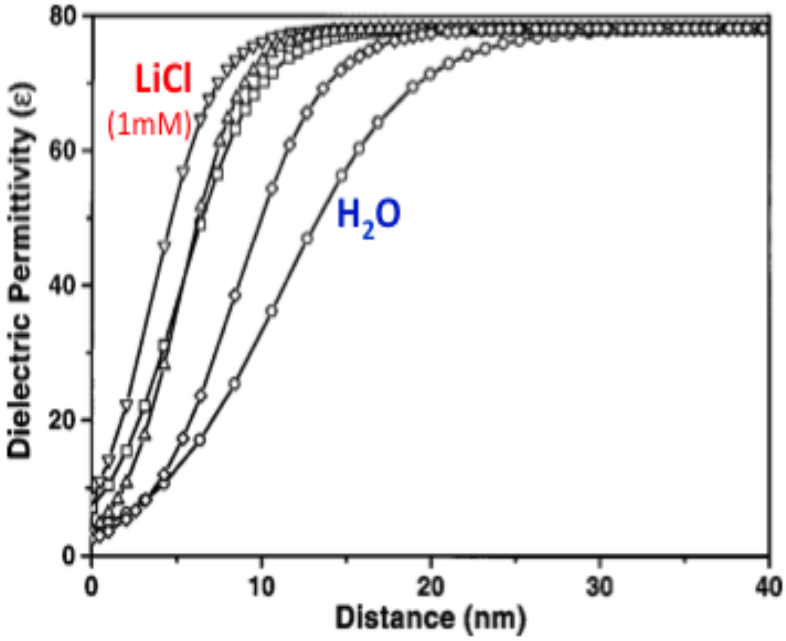

Figure 2 - Variation of permittivity from the electric double layer in a mica-water interface to the interior of the water. The figure shows the variations to pure water and an aqueous solution of 1 mM of lithium chloride [78].

Surface Enhanced Raman Spectroscopy is a more sensible tecnhique than Raman Spectroscopy, being ideal to observe raman spectra with a significant intensity. SERS exhibit an intensification of Raman signal for molecules adsorbed on metallic surfaces 10^5-10^6 times more intense than the same non-adsorbed species [45] and has been widely used to study the adsorption of large groups of molecules including carboxylic acids and amino acids on metal surfaces. In particular, SERS studies [15] suggest that 3-phenylpropionic acid (hydrocinnamic acid) is adsorb on silver surface through the carboxylate group, with the chain of the substituent being extended along the metal surface. Keeping in mind the work of SANS [4], we will look at the interactions between silver colloidal particles with *trans*-cinnamic acid (*t*-CIA) and cyclodextrin molecules and compare native and methylate cyclodextrins behaviours.

CONCEPTUAL FRAMEWORK

1 – COLLOIDAL PARTICLES

1.1 - SODIUM DECANOATE MICELLES

Surfactants (or 'surface active agents') are organic compounds with at least one lyophilic ('solvent-loving') and one lyophobic ('solvent-fearing') group in the molecule. In simplest terms, a surfactant contain at least one non-polar fragment and one polar (or ionic) group. Aggregates of surfactant molecules depend on concentration and shape varying from spherical, to cylindrical and lamellar forms. The aggregation process is called 'micellization' and the aggregates are known as 'micelles'. Micelles begin to form at a distinct and frequently very low concentration known as 'critical micelle concentration' or 'CMC'. In aqueous media, they lead to hydrophobic domains within the solution, whereby the surfactant may solubilize or emulsify particular solutes. Hence, surfactants will modify solution properties at interfaces and in the bulk [63].

As the surfactant concentration increases, the available area at the surface for surfactant adsorption decreases and surfactant monomers starts accumulating in the solution bulk. However, the hydrophobic tail of the surfactant molecules has extremely small solubility in water and the hydrophilic head has extremely small solubility in non-polar solvents. Hence, the hydrophobic effect will drive surfactant monomers to form self-assembled aggregates above certain aggregate concentration. These aggregates are micelles, vesicles, liquid crystals and reverse micelles and exist in equilibrium with the surfactant monomers [53]. The monomer concentration in a micellar solution increases as the total concentration increases and multiple equilibrium is estabilished among monomers, pre-micellar aggregates, and micelles. Relatively small energy is required to overcome the barrier between the monomeric and aggregated states [49].

A study by nuclear magnetic resonance (NMR) proton of the variations in chemical shift of the methyl group of sodium decanoate ($CH_3(CH_2)_8COO^-Na^+$ = NaDec) in deuterated water solutions showed micelle formation with critical micellar concentration [22] approximately equal to 116 mM (Figure 3).

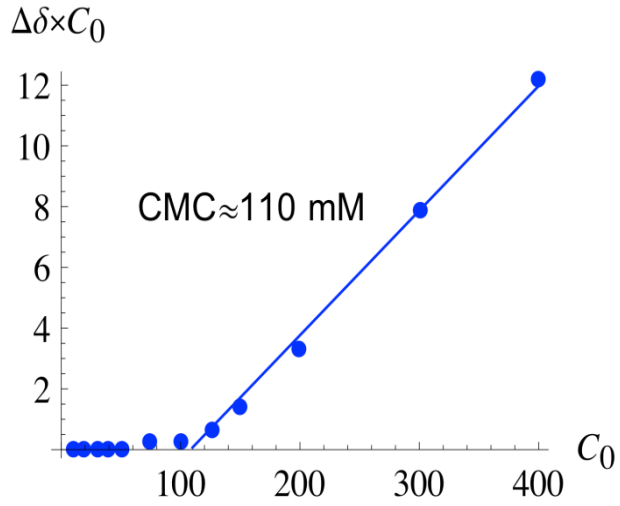

Figure 3 - Variation of the chemical shift of the methyl protons of sodium decanoate Δδ times C_0 = $[NaDec]_0$, $\Delta\delta x C_0$, in function of C_0 [22].

The chemical shift variation Δδ is the difference between the chemical shift of the methyl protons of decanoate anion into the solution as a monomer, and the micelles. The article concludes that the product of Δδ times C_0 is proportional to the concentration of the decanoate monomers in the micelles, C_0 [22]. Hence, below the critical micelle concentration, micelles do not formed (C_n = 0), and above the critical micelle concentration, $\Delta\delta x C_0$ increases linearly with C_0.

1.2 - SILVER NANOPARTICLES

A colloid is a solution that contains particles ranging from 1 and 1000 nanometers in diameter and is still able to remain evenly distributed throughout the solution. They are also known as colloidal dispersions because the colloidal particles remain dispersed and do not settle to the bottom of the container [63].

Metal colloids and colloidal aggregates provide a particularly rich example of local electromagnetic enhancement with several authors suggesting that protrusions on the surface of colloidal particles, lead to giant enhancements of the local field, up to a factor of 10^{14}–10^{15}. Aggregation of metal particles leads to the formation of aggregates with roughness and fractal morphology necessary to render intense Raman spectra [37].

Noble metal (Ag, Au) colloids have been widely employed in Surface Enhanced Raman Specrtroscopy. Among the methods employed to obtain metal colloids the chemical reduction of silver nitrate with citrate [43] produces a more uniform distribution of particle sizes and it was found that SERS intensity increases, as the size of the silver particles becomes larger (average diameter about 50 nm). However, a continuous increase of the particle size (100 – 130 nm) leads to lower SERS intensity signal [64]. Thus, one of the advantages of metal colloids is the possibility to control and modify the particle size and shape by choosing adequate experimental conditions. Silver (Ag) offers two major advantages: SERS enhancement factor is 10 to 100 times higher, and it can be excited from the ultra violet (UV) to the infrared region (IR) [1].

The preparation of silver nanoparticles (Ag_{np}), is commonly done by reducing silver ions in a solution, usually aqueous media, and preventing particle growth by using stabilizing agents such as surfactants and polymers. Citrate and hydroxylamine anions with sodium hydroxide were used as reducing agents at elevated temperatures and the aggregation speed of nanoparticles were controlled by adding chloride anions [42-44].

At ice temperature, borate anions were used to reduce silver ions to produce aggregated silver nanoparticles [21]. In all cases, its important to control the reduction speed by adding anions and/or controlling temperature to produce colloidal solutions [28]. Apart from stabilizing the colloid through steric or electrostatic repulsion, stabilizers also modify the nanoparticles reactivity and functionality depending on their chemical properties and the type of interaction they form with Ag_{np} surfaces.

Silver nanoparticles are found in a wide and diverse range of applications such as photonic and photovoltaic devices, conductive inks or antimicrobial coatings. These nanoparticles also have properties such as a high ability of resistance to oxidation and optical properties [54].

2 – SUPRAMOLECULES AND MOLECULES

2.1 – CYCLODEXTRINS

Cyclodextrins α, β and γ are a family of cyclic oligosaccharides ring-shaped, consisting of 6, 7 and 8 D-glucoses linked by α(1-4) linkages. They are also known as cycloamyloses, cyclomaltoses and Schardinger dextrins. They are produced as a result

of intramolecular transglycosylation reaction from degradation of starch by cyclodextrin glucanotransferase (CGTase) enzyme [82, 26]. In 1903, Schardinger was able to isolate two crystalline products, dextrins A and B, which were described with regard to their lack of reducing power. Schardinger named his crystalline products 'crystallized dextrin α' and 'crystallized dextrin β' [26].

β-cyclodextrin (βCD), a native cyclodextrin, has a homodromic chain (same direction) of hydrogen bonds in the wider edge, even when in aqueous solution. This homodromic chain helps to confer conformational rigidity to the βCD [74]. Apart from these naturally occurring cyclodextrins, many cyclodextrin derivatives have been synthesised. These derivatives are usually produced by aminations, esterifications or etherifications of primary and secondary hydroxyl groups of the cyclodextrins[76, 65].

Figure 4 show representations of cyclodextrin-β (βCD) and heptakis(2,3,6-tri-O-metil)-cyclodextrin-β (TRIMEB). Methylate cyclodextrin has a central cavity that is partially obstructed by a methyl group. The cavities of the cyclodextrins exhibits predominantly hydrophobic characteristics.

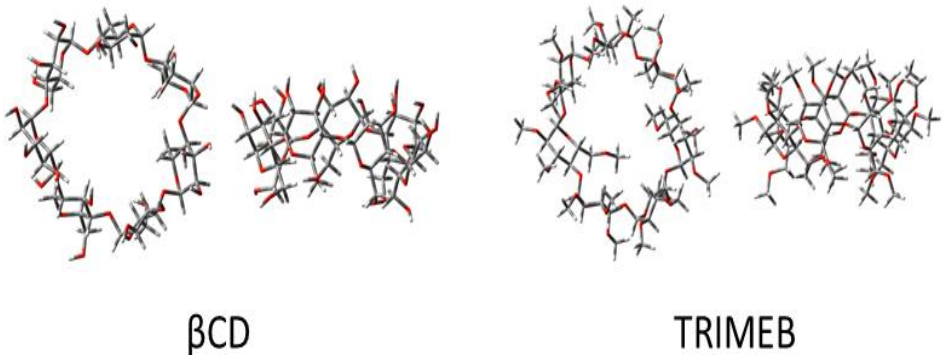

Figure 4 - Cyclodextrin-β and TRIMEB: representations by tubes (red vertices indicate atom O; gray vertices indicate atom C; white extremities indicate atom H) optimized structures in molecular mechanical calculations using the UFF method (Universal Force Field), carried out by system Gaussian09 program.

Figure 5 represents each cyclodextrin by an electronic isodensity surface (= locus of points with the same electron density). This surface it's represented by the electrostatic potential of rainbow colors. A dark red area indicates a high electron density (negative electrostatic potential), while a dark blue area indicates a positively

charged region (positive electrostatic potential). The central cavity has approximately zero electrostatic potential, represented by color green.

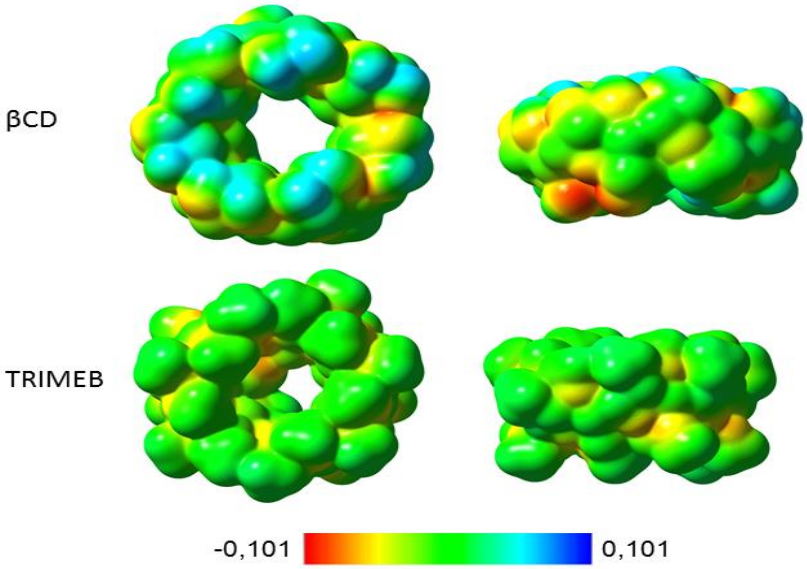

Figure 5 - β-cyclodextrin and TRIMEB: Surface electronic isodensity (isovalue = 0.00040) mapped with electrostatic potentials obtained with software Gaussian09 and calculations using B3LYP / 3-21G // UFF.

Neutron scattering studies revealed that βCD is strongly rigidified by intramolecular hydrogen bonds between the secondary hydroxyl group of adjacent anhydroglucose unit, leading to a very low aqueous solubility (1.85% w / v, 25° C) [85, 80]. The conformational stabilization of βCD is lost upon replacement of the OH groups for the CH_3, methylate cyclodextrins are less hydrated than the native ones [88]. The water solubility coefficient is positive for natural CDs, because solubility increases with temperature but is negative for methylate CDs, which are more soluble in cold water than in hot water where they crystallize [39].

2.1.1 - Cyclodextrin – guest interaction

In aqueous solution, cyclodextrins and their derivatives are specially known for their ability to form inclusion complexes with reversible nonpolar molecules (Figure 5). The inclusion of a guest molecule in the cyclodextrin cavity consists of replacing some or all water molecules within the cavity by the guest molecule whose dimensions fits the cavity [76]. In the cyclodextrin interior can occur polar - apolar, Van der Waals and

electrostatic interactions. The inclusion of a guest molecule into cyclodextrin cavity can be measured by a constant inclusion, K_a [19, 33, 75].

The cyclodextrin – guest inclusion complex is a function of two key factors. The first is steric and depends on the size of the cyclodextrin, the guest molecule and also the functional groups within the guest and the second critical factor being thermodynamic interactions between the different components of the system (cyclodextrin, guest, solvent). For a complex to form there must be a favorable net energetic driving force that pulls the guest into the cyclodextrin [24].

Researchers have studied the formation of the inclusion complex of some molecules, but few studies include conclusive techniques for confirmation of the inclusion complex. Only nuclear magnetic ressonance spectroscopy has been used to provide conclusive information at molecular level. However, Raman Spectroscopy, Fourier Transform Raman Spectroscopy (FT-Raman) and Fourier Transform Infrared Spectroscopy (FT-IR) are considered excellent tools for studying the formation of inclusion complex.

2.2 - CINNAMIC ACID

The molecule, *trans*-cinnamic acid, is mostly found naturally in many spices such as cranberries, prunes, cinnamon, and cloves; provides a natural protection against pathogenic organisms [16] and has a great medicinal interest through their anti-inflammatory, anti-tumoral and antioxidant properties. Storage conditions such as temperature, light, and pH should be controlled and kept constant to ensure the least amount of variability [23].

Cinnamic acid is a lipophilic weak acid and is slightly soluble in aqueous solutions, due to the fact that contain a propenoic chain, which results in a poor solubility and low bioavailability. Cyclodextrins can be used to improve the solubility and stability of *trans*-cinnamic acid. The constant inclusion of *t*-CIA change in the presence of cyclodextrins due to diameter of cyclodextrins[18].

Organic compounds with an aromatic ring have a favoured interaction with the cyclodextrin cavity and are suitable guest molecules to include in CDs [9, 10, 62].

Cinnamic acid in addition to an aromatic ring present a carboxyl group that allows the occurrence of hydrogen bonds interaction with hydroxyl group of CDs[8].

Experimental results using dissolution studies and thermal gravimetric analysis demonstrated that cinnamic acid form an equimolar ratio of 1:1 stoichiometric inclusion complex with βCD by non-covalent bonds [79]. Nuclear magnetic ressonance studies have shown slight changes with the guest and host when complex formation occurs. Protons (H-3 and H-5) within the cyclodextrin cavity shift to a higher field when complexed with cinnamic acid. These chemical shifts suggest that phenyl group is inside the cyclodextrin cavity (Figure 6) [81].

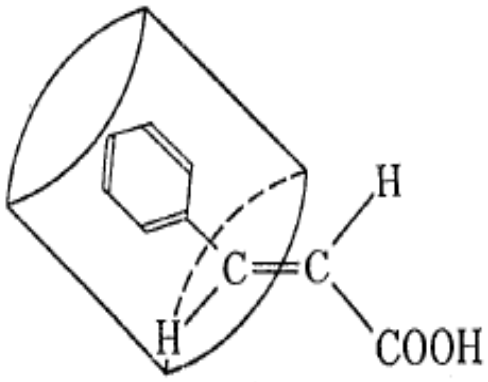

Figure 6. Proposed Structure of Inclusion Complexes of Cyclodextrins with Cinnamic Acids [81].

Cinnamic acid and α-cyclodextrin, (αCD), complement one another in size and shape, yielding a complex that is effective and produces higher magnitudes of extrinsic optical activity. Within the inclusion complex, the diameter of αCD is smaller and better host the cinnamic acid due to the benzene ring, as compared to the others cyclodextrins [81]. Benzene ring will fit in both α and β cyclodextrin as their interiors range from 6 to 8 Å.

3 – VIBRATIONAL SPECTROSCOPY

3.1 - RAMAN SPECTROSCOPY

In Raman Spectroscopy the sample is irradiated with a laser and the diffused light is normally seen in the perpendicular direction to the incident beam. The diffused light has two sources: one is called Rayleigh diffusion, formed by radiation with the same

frequency as the incident beam; another, called Raman diffusion, which is very low (~10^{-5} of the incident beam) and have frequencies $\nu_0 \pm \nu_m$, where ν_m is the molecule vibrational frequency. The lines $\nu_0 - \nu_m$ and $\nu_0 + \nu_m$ are called anti-Stokes and Stokes, respectively. Thus, Raman spectrum is typically recorded in Stokes region, being Raman shift ν_m, on the horizontal axis of the spectrum (Figure 7) [29].

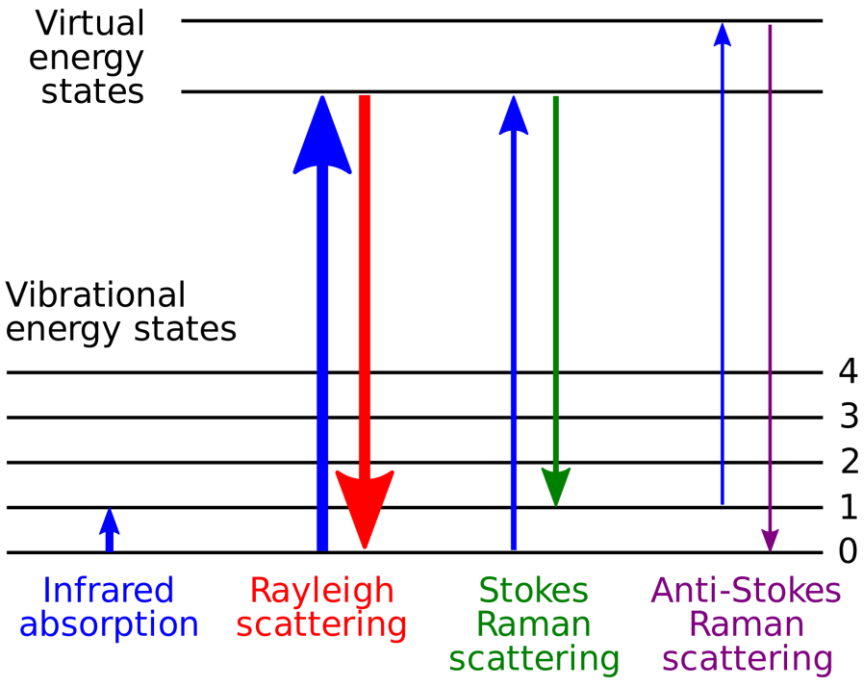

Figure 7. Electronic - vibrational energy states diagram involved in Raman Spectra [61].

The Raman effect consists on the inelastic scattering of monochromatic light from a laser. The electrical field of the incident radiation on sample induce a dipole moment in the molecule [45]. The relationship between the induced dipole moment and the electric field is established by polarizability, α, of the molecule trought the equation

$$\vec{\mu}_{ind} = \alpha \vec{E}$$

In a molecule the polarizability tensor is represented with a cartesian axis system, a 3x3 matrix with matrix elements α_{xx}, α_{xy}, α_{xz}, α_{yx}, α_{yy}, α_{yz}, α_{zx}, α_{zy}, α_{zz}. Generally, this matrix is real and symmetric. In the equation above, the electric field of the radiation is oscillatory and the induced dipole moment is also oscillating. For a

active Raman vibration, the polarizability must present a non-zero variation on the coordinated vibration, where Q_i represent the coordinate *i* of the molecule vibration.

$$\frac{\partial \alpha}{\partial Q_i} \neq 0$$

Raman spectroscopy is particularly sensitive to weak interactions. To understand this statement, it should be recognized that, in general, weak interactions are dispersion interactions, resulting from induced dipole - induced dipole interactions [45]. Considering the interaction system of two atoms, the energy dispersion is approximately given by expression London,

$$E_{AB}^{disp} \approx -\frac{3}{2}\frac{I_A I_B}{I_A + I_B}\frac{\propto^A \propto^B}{R^6}$$

where I_A e I_B are the first ionization energy of the atoms A and B, R is the distance between them. The energy dispersion depends on the polarizabilities wich also influence the intensities of Raman bands in the spectrum.

Raman spectra have on the ordinates axis Raman intensities and on abscissa, the Raman shifts, commonly expressed in wavenumbers (unit cm^{-1}). The most important frequencies for identification of organic compounds occur in the region of 4000 to 1300 cm^{-1}. In this region we know the functional groups present in the unknown substance. The region of lower frequencies, 1300-250 cm^{-1}, is often called the fingerprint region, and the lines observed in the spectrum are the characteristics of the molecule as a whole. The origin of these spectral lines is complex, involving vibrations of angular deformation, vibrations between the same or similar masses. Although, the angular vibration can present values that allow diagnoses, most of them are strongly influenced by changes in the rest of the molecules [77].

There are many advantages and disadvantages in Raman Spectroscopy. Referring to Resonance Raman effect (RR) is possible to selectively increase the vibration intensity of a particular group in the molecule. This is particularly advantageous in vibrational study of biological molecules that possess a chromophoric group. Since the diameter of the laser beam is normally 1-2 mm, only a small area of the sample is required to obtain Raman spectra [29].

Since water is a weak diffuser, Raman spectra for aqueous samples can be obtained without much interference of water vibrations. Thus, Raman spectroscopy is ideally suited for biological studies of compounds in aqueous solution. Raman spectra of hygroscopic compounds and / or air sensitive may be obtained by placing the sample in a sealed glass tube, the region of 4000 to 50 cm^{-1} can be withdrawn all together.

Despite its great use, this spectroscopy has some disadvantages [29]. The use of a laser as a radiation source cause heating and / or photo-decomposition of the sample, especially in Raman Spectroscopy where the laser frequency is deliberately "tuned" on absorption band of a molecule. Another disadvantage is the presence of fluorescence that obscures or hinders the observation of Raman bands [29].

While Raman spectra are normally associated with vibrational transitions in liquids and solids, is possible to record a Raman spectra associated with electronic transitions between minimum and excited energy states. The difusion of Resonance Raman occurs when the excited state involve intercepts energy of multiple excited electronic state. In liquid and solid, vibration levels are extended to produce a continuum whereas in gaseous state, there's a series scale of discrete levels [77].

Raman Spectroscopy has advanced tremendously in recent years and has increased applications in pharmaceutical industry. Raman spectra of cyclodextrins present free regions of bands that can be used as windows for monitoring relevant guest modes, such as stretching vibration of double bonds (C=C), (C-O) and aromatic (C-H) bonds [67].

3.2 - SURFACE ENHANCED RAMAN SPECTROSCOPY

Surface Enhanced Raman Spectroscopy was first documented in 1974 when Fleischamn et al [30] demonstrated that Raman signal of pyridine adsorbed on an electrochemical roughened silver electrode was many times greater than expected. Because the voltage applied to the electrode affected the signal level it was attributed to an increased surface coverage of pyridine on electrode. A few years after, Van Duyne et al [38] managed to quantify the phenomenon and found an enhancement or increase in Raman cross section of the adsorbed pyridine molecules. This, lead to conclude that the increase of the

Raman signal was due to an unique electromagnetic environment present in the roughened silver in which pyridine was adsorbed [38].

Numerous other observations [25, 41, 57] were made in the subsequent years in order to understand the electromagnetic explanation for Raman enhancement, which became universally known by the acronym SERS [48], stand for Surface Enhanced Raman Spectroscopy. Since its discovery in 1974, SERS has become widely used, offering many advantages over other techniques such as FT-IR Spectroscopy, Ultra Violet-Visible-Near Infrared (UV–vis-NIR) Absorption, X-Ray Photoelectron Spectroscopy, Mass Spectrometry and others [71].

A plasmon resonance is a core process in SERS and mostly silver (Ag) and gold (Au) metals are used as substrates because of surface plasmon resonance in visible region. Metals like Al, Ga, In, Pt, Rh, and alkali metals (Li, Na, K, Rb and Cs) can also be used as substrates in SERS but enhancement is low compared to Ag and Au [68].

The use of some metal colloids allows to study the adsorption of many organic molecules. Its highly sensitivity permits an accurate structural study of many molecules at very low bulk concentrations. The first study carried out on saturated aliphatic acids was by Moskovits and Suh, which focused on the SERS spectra on silver hydrosols of monocarboxylic (from valeric to decanoic) and dicarboxylic (from oxalic to suberic) acids [51]. The intensity observed in SERS usually exceeds by a factor of 10^5–10^6 and in special cases 10^{12}–10^{14} is observed in normal Raman scattering. Moreover, the SERS effect becames even stronger if the frequency of excitation light its in resonance with absorption band of the molecule [37].

3.2.1 - Electromagnetic Enhancement Mechanism

Surface Enhanced Raman Scattering is a complex phenomenon capable of producing an enormous enhancement of Raman signal of some molecules adsorbed on the surface of some metals, specially silver. Over the years, groups have aimed to maximize the enhancement factor (EF), with reporting numbers as high as 10^{14} [46].

SERS obey two different rules, electromagnetic enhancement mechanism (EM) that study the strengthening or weakening of specific Raman/SERS bands in order to decide the molecular orientation and geometrical configuration of the adsorbed species

on metal surface. The selection rules of EM relate to perpendicular or parallel orientation of planar molecules with respect to the surface, with a consequent enhancement of in-plane or out-of-plane normal modes, respectively [52]. The electromagnetic mechanism suggest that electromagnetic resonance of the metal nanoparticle (now termed localized surface plasmon resonance) underpins the enhancement and it's independent of bonding between the analyte and the metal surface [36]. Using theoretical frameworks, this electromagnetic mechanism can be used to explain enhancement factors of 10^4-10^8, and depends approximately on magnitude of the incident electric field [$E(\omega)$] raised to the fourth power,

$$EF_{EM} \propto |E(\omega)|^2 |E(\acute{\omega})|^2 \approx |E(\omega)|^4$$

E(ω) is the frequency-dependent electric field at incident frequency ω, and E(ώ) is the frequency-dependent electric field at Stokes shift frequency ώ. From this equation the maximum EF_{EM} lie between the plasmon frequency and the Stokes frequency. The Stokes shift is normally small relative to the frequency of the laser; therefore the equation is usually approximated as,

$$EF_{EM} \propto |E(\omega)|^4$$

There is a small enhancement in Raman intensity compared with absence of surface, on the order of a factor of 10 or less for metals like Ag, arising primarily from coherent superposition of the incident and reflected fields at position of the molecule doing the scattering [66]. If the surface under consideration is roughened, then the electrodynamics of irradiated surface become much more interesting. The key is that surface plasmons can now be excited by electromagnetic radiation, resulting in enhanced electromagnetic fields close to the surface (Figure 8) [66].

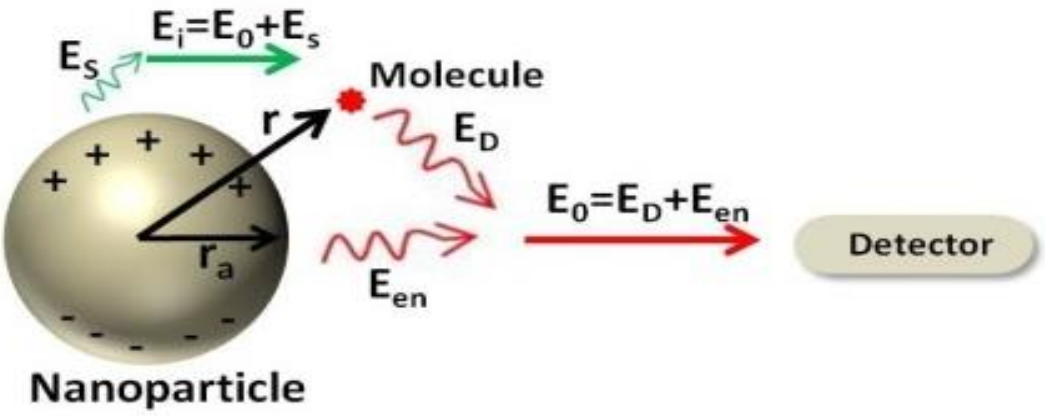

Figure 8. Electromagnetic Enhancement Mechanism. The metal nanoparticle experiences a electromagnetic field E_0 which produces an oscillating dipole moment in the nanoparticle [69].

3.2.2 - Chemical Enhancement Mechanism

However, the fact that chemical enhancement mechanism (CM), is nowadays recognized as general in SERS, it doesn't account for the selective enhancement of bands with the same symmetry which, in turn, could be explained throught the presence of charge transfer (CT) enhancement process [5]. Chemical enhancement accounts for 10-100 (relatively small, but nevertheless important) of the total enhancement factor and requires the molecule to be in direct contact (bonded) with the surface of the metallic nanostructure [13]. These are strongly dependent on the nature of the molecule, the metal and the particular experimental conditions, and can be envisaged as a resonant photo induced electron transfer process between the metal and the molecule.

The charge-transfer mechanism occurs when the wave functions of the molecule and the metal overlap. In this case, the enhancement process occurs in a five-step method. First, the metal absorbs the photon and excites the surface plasmon resulting in a hot electron state. The hot electron gets transferred to the lowest unoccupied molecular orbital (LUMO) of the molecule. The increase in LUMO electrons leads to an increased of Raman signal due to a bigger probability of electron-phonon coupling in the Raman scattering tensor. The energy is then transferred to the molecule, which is used to excite the molecule into an excited electronic state. The molecule relaxes and the energy is transferred back to the metal, from the LUMO, which in turn re-radiates the new photon with Stokes shifted frequency.

Despite solid theoretical modeling, this mechanism remains controversial because of the difficulty in experimentally isolating charge transfer contributions (Figure 9) [50].

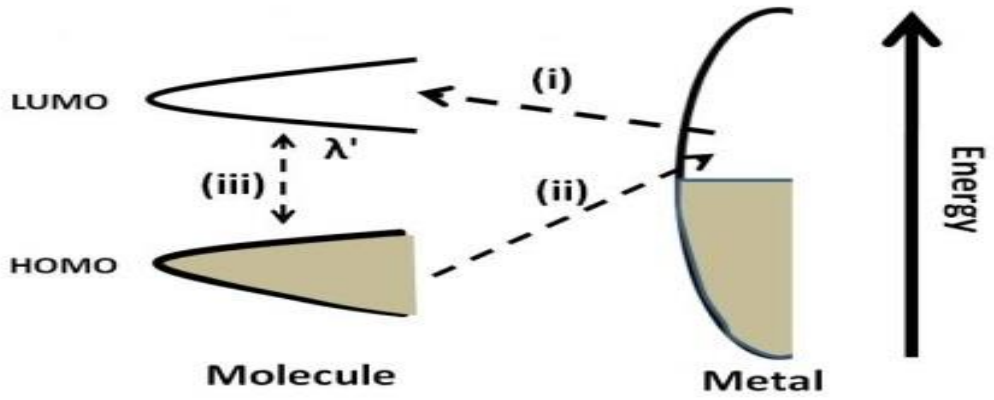

Figure 9. Chemical Enhancement Mechanism. HOMO and LUMO interact with the metal surface and are broadened into resonances [69].

Chemical mechanism is similar to Resonance Raman and therefore an electron is transferred from the Fermi level of the metal to vacant orbitals in adsorbate, for which the excited state would be equivalent to radical anion of these neutral molecules. Therefore, the resonance condition is determined by the position of the Fermi level and by the energy of incident photon [6].

Resonance Raman differs from normal Raman in a way that molecule is able to absorb the incident radiation through normal electronic absorbance transition and occurs a conventional electronically excited state. In this mechanism the relatively narrow-band Raman spectrum superimposed upon the fluorescent emission band of the molecule is often observed [70]. However, since there's fluorescent emission that is proportional to square root of intensity of fluorescent signal, this method is often used. On the other hand, when fluorescent emission is suppressed, either by quenching through proximity to a metal surface or in other time-resolved motifs, then electronic resonance contribute substantially to detectability of Raman signal [35].

Some chemical transformations or decompositions of different types have been reported in SERS experiments, such as polymerizations, isomerizations, photodecompositions and hydrolysis reactions [20].

CM isn't usually considered when analyzing a SERS spectrum. This is probably because of a rather complex effect occurring at atomic or nanometric scale and related to transitions between the ground electronic state of the adsorbate-metal (A-M) system and charge transfer excited levels. These electronic transitions of the surface complex are very difficult to be observed directly [7].

EXPERIMENTAL SECTION

1. MATERIALS AND METHODS

1.1 – RAMAN SPECTRA

1.1.1 - Materials

Sodium decanoate (NaDec, Sigma, 98%), water Milli-Q, β-cyclodextrin (βCD, Aldrich, 97%) and heptakis(2,3,6-tri-O-metil)-β-cyclodextrin (TRIMEB, CycloLab 99,5%).

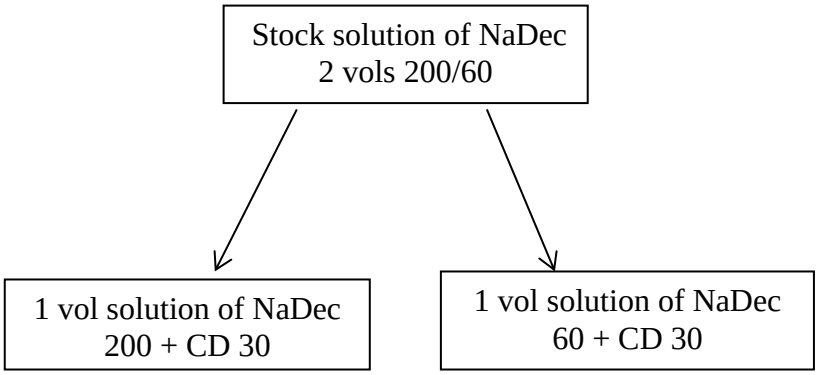

Figure 10 - Procedure for preparing the solutions (schematic). Numerals stand for concentrations (mM).

1.1.2 - Samples

Milli-Q water was used in the preparation of all solutions and mixtures. All glassware was carefully washed with ethanol and dried before use. Five ml volumes of 60 mM and 200 mM sodium decanoate solutions were prepared by slow addition of appropriate amounts of sodium decanoate to Milli-Q water, with constant stirring. Each of these solutions was divided in two equal volumes and appropriate amounts of cyclodextrin (βCD or TRIMEB) were added to each of them to obtain solutions 30 mM in the cyclodextrin.

The following aqueous solutions were obtained: 60 mM and 200 mM in sodium decanoate (D60 and D200), 30 mM in the cyclodextrin (βCD or TRIMEB), 30 mM in the cyclodextrin and 60 mM in sodium decanoate (B30D60 and T30D60) and 30 mM in the cyclodextrin and 200 mM in sodium decanoate (B30D200 and T30D200).

While the solubility of βCD at room temperature in water is 1.85 g/100 mL [80], that is, *ca*. 16.3 mM, its solubility in excess of sodium decanoate is far greater due to the formation of the inclusion complex, thus making possible to prepare the above sodium decanoate aqueous solutions 30 mM in βCD, at room temperature (Figure 10).

1.1.3 - Raman Spectrometer

Raman spectra (Figure 11) were obtained at room temperature (20-21ºC), with a T64000 triple stage spectrometer in the double subtractive plus spectrograph configuration (focal distance 0.640 m, aperture f/7.5, holographic gratings of 1800 grooves mm^{-1}). A 90º geometry between the incident radiation and the collecting system was employed. The entrance slit was set to 200 μm and the intermediate slit between premonochromator and spectrograph was set to 30 mm. The detection system was a liquid nitrogen cooled non-intensified 1024 x 256 pixel (1") charge coupled device chip. The 514.5 nm line of an Ar^+ laser (Coherent, model Innova 300-05) was used as excitation radiation, providing ca. 15 mW at the sample position. The samples were sealed in Kimax capillary tubes of 0.8 mm inner diameter. The spectra were collected with an acquisition time of 60 s for 10 accumulations. Under the above conditions, the error in the determination of frequencies is estimated to be 1 cm^{-1}.

The Raman spectrometer control and data processing were performed using the LabSpec 5.0 (Horiba, France) software, that carry out baseline corrections to the spectra, apply a scaling factor to the band intensities of a spectrum, add and subtract data. All spectra were recorded from 300 cm^{-1} to 3800 cm^{-1} and a polynomial baseline correction of degree 6 was applied.

Figure 11 - Jobin Yvon T64000 spectrometer-triple monochromator.

Source: Vibrational Laboratory from Molecular Physics and Chemistry Department of University of Coimbra.

1.1.4 - Frequency Calculations

Frequency and Raman intensity calculations were performed by the system of programs *Gaussian* 09 [31], with the B3LYP DFT method and the 6-31 + G(d,p) basis set, the frequencies being scaled by the factor 0.964 ± 0.023 [55]. Optimized geometries for the inclusion of decanoate ion in βCD and in TRIMEB were treated with the ONIOM method for two layers, the high layer being composed by the decanoate ion and one glucosidic unit of the cyclodextrin and treated at the B3LYP/6-31 + G(d,p) level, the low level being taken at the Molecular Mechanics UFF method. In the absence of interglucose hydrogen bonds, TRIMEB shows a somewhat distorted macrocycle. Tables 1 and 2 present the calculated (scaled) frequencies (cm^{-1}) of peak intensities in the CH stretching region, their approximate descriptions and the observed frequencies.

Table 1. Calculated (scaled) frequencies (cm^{-1}) of peak intensities, in the CH stretching region, for the 1:1 inclusion complex of decanoate ion in βCD (Glu=glucose unit; s=symmetric, as=antisymmetric), and observed Raman shifts for the B30D200 spectrum.

Glu_Dec	approx.description	observed Raman shifts / cm^{-1}
2854	(Glu) CH	2856
		2875
2889, 2907	(Dec) CH_2 s	2902
2918	(Glu) CH_2 s + (Dec) CH_3 s	2920
2934	(Dec) CH_2 as	2939
2951	(Glu) CH + (Dec) CH_2 as	
2982	(Dec) CH_3 as	2970
2996	(Glu) CH_2 as	2999
3005	(Glu) CH	

Table 2. Calculated (scaled) frequencies (cm^{-1}) of peak intensities, in the CH stretching region, for the 1:1 inclusion complex of decanoate ion in TRIMEB (Tmg=trimethylglucose unit; s=symmetric, as=antisymmetric), and observed Raman shifts for the T30D200 spectrum.

Tmg_Dec	approx.description	observed Raman shifts / cm^{-1}
2857	(Tmg) CH_3 s	2857
2882, 2889	(Tmg) CH_2 s, (Dec) CH_2 s	2889
2902	(Tmg) CH_3 + (Dec) CH_2 s	
2917, 2927	(Dec) CH_2 s	2931
2935, 2948	(Dec) CH_2 as	2943
2953, 3053	(Tmg) CH	
2982	(Dec) CH_3 as	
3009, 3013	(Tmg) CH_3 as	3008

1.1.5 - Spectra Decomposition in Lorentzian-Gaussian Functions

Raman spectra between 2700 cm^{-1} and 3100 cm^{-1} were decomposed using *Mathematica* [87] as the linear combination $a\,L + (1 - a)\,G$, where

$$L(\nu) = I_{max} / [\,\alpha\,(\nu - \nu_{max})^2 + 1\,] \qquad G(\nu) = I_{max} \exp[-\beta\,(\nu - \nu_{max})^2\,]$$

represent Lorentzian and Gaussian band shapes (I_{max} and ν_{max} are the intensity and frequency at the maximum) and a represents the fraction of the Lorentzian character (1-a is the fraction of Gaussian character). In this fitting, the variable parameters were the Raman shifts at the maxima, the intensities at zero shifts, full widths at half height (FWHH) and the a parameters. The Raman shifts at the maxima were initially set by trial and error, followed by the fitting of the FWHH values and intensities at zero shifts. The a parameters were fitted at last.

1.2 – SURFACE ENHANCED RAMAN SPECTRA

1.2.1 - Materials

Water milli-Q, β-cyclodextrin (βCD, Aldrich, 97%), heptakis(2,3,6-tri-O-metil)-β-cyclodextrin (TRIMEB, CycloLab 99,5%), silver nitrate ($AgNO_3$), sodium borohydride ($NaBH_4$), sodium sulfate (Na_2SO_4), sodium hydroxide (NaOH), hydroxylamine hydrochloride ($NH_2OH.HCl$), *trans*-cinnamic acid (*t*-CIA, Sigma-Aldrich, 97%).

1.2.2 - Colloid Preparation

The sodium borohydride colloidal solution was prepared with Milli-Q water according to the method described by Creighton et al [21]. Consist of reducing an aqueous solution of 10^{-3} M $AgNO_3$ with an excess of $NaBH_4$. To this end, 10 mL of 10^{-3} M $AgNO_3$ was drop wise added with stirring to 30 mL of previously cooled $2x10^{-3}$ M $NaBH_4$. After vigorously stirring the mixture for about one hour, the initial dark colour was gradually replaced by a yellow colour (Figure 12) which is an indication of a colloidal solution. The mixture was allowed to rest at room temperature for one day.

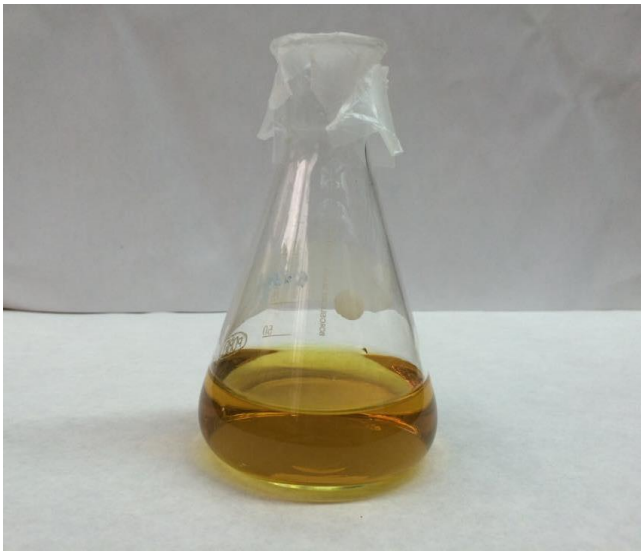

Figure 12. Silver borohydride colloidal solution.

The hydroxylamine colloid solution [44] consists of reducing an aqueous solution of 10^{-2} M $AgNO_3$ with an excess of $NH_2OH.HCl$. To this end, 10 mL of 10^{-3} M $AgNO_3$ was drop wise added with stirring to 90 mL of $1.66x10^{-3}$ M $NH_2OH.HCl$. Before adding AgNO3, 300 μL of NaOH 1M was added to the solution of $NH_2OH.HCl$ to control the pH solution. After vigorously stirring the mixture, a gradually dark yellow colour appeared (Figure 13) which is an indication of a colloidal solution. The mixture was allowed to rest at room temperature for one day.

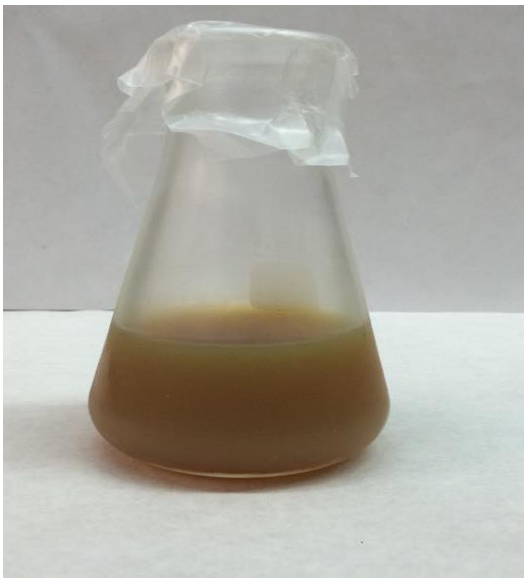

Figure 13. Silver hydroxylamine colloidal solution.

1.2.3 – Samples

Stock solution of *t*-CIA with concentration 30 mM was prepared for a volume of 10 ml, 5 ml of Milli-Q water and 5 ml of sodium hydroxide 1M. Cinnamic acid reacted with sodium hydroxide to give sodium *t*-cinnamate and water, according to

$$t\text{-CIA} + Na^+OH^- \rightarrow Na^+t\text{-}CI^- + H_2O$$

After the stock solutions were prepared, 700 μL of CD were removed, placed in an eppendorf and added to 700 μL of *t*-CIA (Figure 13). This combined solution is 15 mM in *t*-CIA and 15 mM in CD, with the acid in a ratio of 1 *t*-CIA : 1 CD. Then, 10 μL of *t*-CIA and *t*-CIA_CD were removed and added to the colloidal solution. After

a while a change in colour was observed. The effect of time in the colloidal solutions were studied and observed its influence on the recorded spectra

.

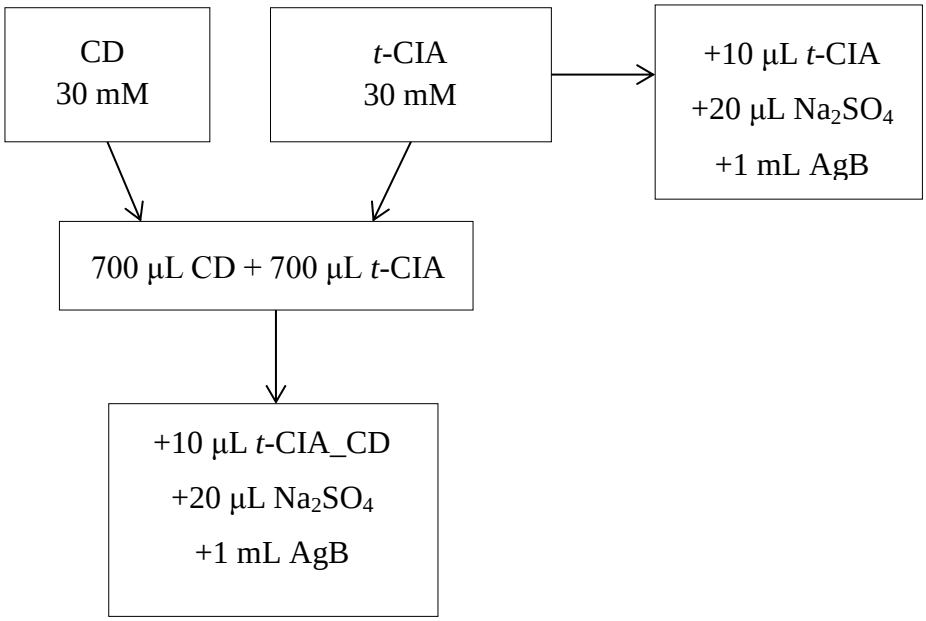

Figure 14. Procedure for preparing the solutions (schematic).

1.2.4 - UV-VIS Spectrophotometer

Absorption spectrum of silver colloid borohydride (Figure 12) was obtained with an Agilent 8453 diode array spectrophotometer over a wavelength range of 300-800 nm. UV/visible spectrum of colloidal solution was obtained by pipetting 500 µL of the colloid into a quartz cuvette and adding 1 mL of water. The spectrum contained a strong plasmon band close to 396 nm, which confirms that silver ions were reduced to Ag^o in the aqueous phase (Figure 15).

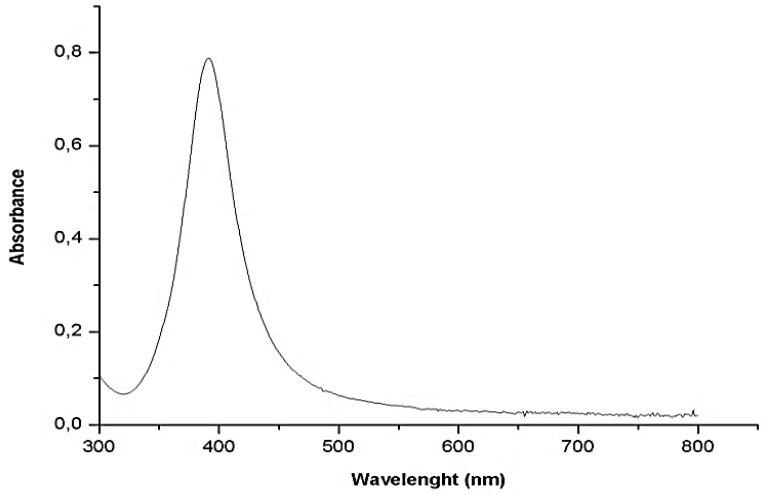

Figure 15. UV-Vis absorption spectrum of yellow silver colloid borohydride.

1.2.5 - Raman Spectrometer

The spectra were recorded from 300 cm^{-1} to 3200 cm^{-1} with a Renishaw Reflex inVia Raman macrospectrometer coupled to a RenCam CCD (Charged Coupled Device) detector (Figure 16). The 514.5 nm line from an argon laser was used as the exciting radiation. A quartz cell with a 1 cm path length was also used. The objective of macro system at 90º had a focal distance of 30 mm^{-1} and a numerical opening of 0.17.

Figure 16. Invia Reflex Raman (RENISHAW) microscope.

Source: Laboratory from Physics and Chemistry Department of University of Malaga.

RESULTS AND DISCUSSION

1 – RAMAN SPECTROSCOPIC EVIDENCE FOR THE INTERACTION BETWEEN TRIMETHYL-β-CYCLODEXTRIN AND SODIUM DECANOATE MICELLES IN WATER

1.1 - RAMAN ABSOLUTE INTENSITIES

The absolute intensity of a Raman signal at the scattered radiation frequency ν is given by

$$I\ (\nu) \propto K\ (\nu)\ x\ \nu^4 x\ P_0\ x\ C$$

where $\propto$ means "proportional to", $K(\nu)$ is the spectrometer response function that depends on the scattered radiation wavelength through the instrument optics, gratings, filters, polarisation and detector, $S(\nu)$ is a sample specific factor that represents the scattering properties of the sample like the Raman cross-section and the scattering volume, P_0 is the laser power density at the sample position and C is the sample concentration [32]. Multiplication of a whole Raman spectrum [the complete list of $I(\nu)$ values] by a non-zero constant does not affect the ratio of integrated intensities of Raman bands in the same Raman spectrum, only changes the arbitrary scale of intensity units.

1.2 - THE RAMAN OH STRETCHING BAND OF WATER AS AN EXTERNAL INTENSITY STANDARD

The Raman spectrum of liquid water (Appendix 1) has been the subject of a number of previous studies [14, 58, 73, 83, 84]. In particular, the Raman feature between 300 cm^{-1} and 1000 cm^{-1} with maximum at *ca.* 470 cm^{-1} is composed by three Raman active intermolecular librational modes [14]. In turn, the HOH bending Raman, whose maximum occurs nominally at 1640 cm^{-1}, has a slightly asymmetric band shape that suggests being composed by two distinct components [14]. At last, the Raman bands between 2700 cm^{-1} and 3800 cm^{-1} are assigned to the OH stretching modes [58, 73, 85].

In diluted aqueous solutions, at ambient temperature, the water solvent concentration is approximately equal to 55.5 mol dm^{-3}, as the densities of diluted aqueous solutions do not appreciably depart from the density of pure water approximately given by 1.00 g/cm^{-3} [34]. In diluted aqueous solutions, the solvent concentration greatly exceeds the solute concentration and the Raman bands of water that correspond to group frequencies (the HOH bending and the OH stretching bands) can in principle be used as external standards to normalize the Raman spectrum of a diluted aqueous solution. In particular, the Raman HOH bending band is exclusively associated with the water solvent. However, this is a very weak, broad and asymmetric Raman band, sometimes lacking a well defined baseline due to interference with nearby Raman and fluorescence bands. Hence, its use as an external intensity standard can lead to appreciable errors.

In turn, the Raman OH stretching bands of liquid water are very strong and can be used as an external intensity standard for normalization of the Raman spectrum of a diluted aqueous solution. Raman OH stretching bands of aqueous solutions have been previously used as internal standard in a number of studies. In addition, various methods for calibrating Raman intensities have been described [47, 72] and a comprehensive review of phtotometric standards for Raman spectroscopy is found in [59].

1.3 - EQUILIBRIUM CONCENTRATIONS

The cyclodextrin and sodium decanoate aqueous solutions, B30D60, B30D200, T30D60 and T30D200, have the inclusion complex in dynamic equilibrium with the cyclodextrin and the decanoate ion in aqueous solution. Before we obtain the Raman spectra referring to the 1:1 inclusion complexes, all the decanoate and cyclodextin concentrations in solution need to be determined.

Conservation of the total cyclodextrin and decanoate concentrations is expressed by the following equations

$$[CD]_t = [CD] + [CD\_D]$$

$$[D]_t = [D] + [CD\_D]$$

where

$$[CD\_D] = K[D][CD]$$

and D and CD stand for decanoate and cyclodextrin respectively, *K* represents the binding inclusion constant, [D] stands for the decanoate concentration in solution and in the micelles (there are equilibria involving these concentrations) and [CD_D] stands for the concentration of the 1:1 inclusion complex.

According to the preparation of the aqueous solutions, the total concentrations are $[CD]_t$ = 30 mM, $[D]_t$ = 60 mM for B30D60 and T30D60, and $[D]_t$ = 200 mM for B30D200 and T30D200. For the decanoate ion inclusion in βCD, the binding constant obtained by affinity capillary electrophoresis is $3.7x10^3$ [47]. Using this value, the mathematical solution of the two equations yields [βCD_D] ≈ 30 mM as there is an excess of the decanoate concentration over the cyclodextrin concentration, [βCD] ≈ 0, [D] ≈ 30 mM and [D] ≈ 170 mM for B30D60 and B30D200 respectively.

For the decanoate ion inclusion in TRIMEB, a binding constant value could not be found in the literature. However, using trial binding constant values equal to 10^i for i = 1, 2, 3, 4, the concentration values are approximately equal to those found for the βCD aqueous solutions. The cyclodextrin and sodium decanoate aqueous solutions, B30D60, B30D200, T30D60 and T30D200, have an excess of sodium decanoate over the corresponding cyclodextrin and the cyclodextrin concentrations in solution are negligible.

1.4 - RAMAN SPECTRA FOR THE 1:1 INCLUSION COMPLEXES

In order to obtain the Raman spectrum due to the 1:1 inclusion complex, we need to deal with spectra that share a common intensity scale. To this end, we start by taking the Raman OH stretching bands of Milli-Q water as an external standard. The Raman spectrum of one aqueous solution is normalized when the profile of its complex of Raman OH stretching bands matches as closely as possible the Raman OH stretching bands of Milli-Q water. Being impossible to obtain a perfect match in all Raman shifts, preference is given to the match on the lower wavenumber wing of this complex of bands, so that CH stretching bands become free from overlapping with the wing of the

OH stretching bands. After spectral normalization, we can proceed to subtract the water spectrum.

These considerations can be easily applied to the inclusion of decanoate ion in TRIMEB. Considering the aqueous solution with a total decanoate ion concentration equal to 200 mM and TRIMEB concentration equal to 30 mM. Figure 17 illustrates the normalization of the Raman spectrum of the aqueous solution T30D200 with the Raman OH stretching bands of Milli-Q water and shows the Raman spectrum resulting from the subsequent subtraction of the Raman spectrum of Milli-Q water, the same procedure was made to T30D60, B30D200, B30D60, D200 and D60 (Appendix 2).

We represent this Raman spectrum by T30D200ns, where "n" and "s" stand for normalization and subtraction of the water solvent. As an order of magnitude of the error involved in the spectral normalization, the integrated intensity of the residual OH stretching bands in the T30D200ns spectrum amounts to 4.0 % of the integrated intensity of the complex of the OH stretching bands of Milli-Q water

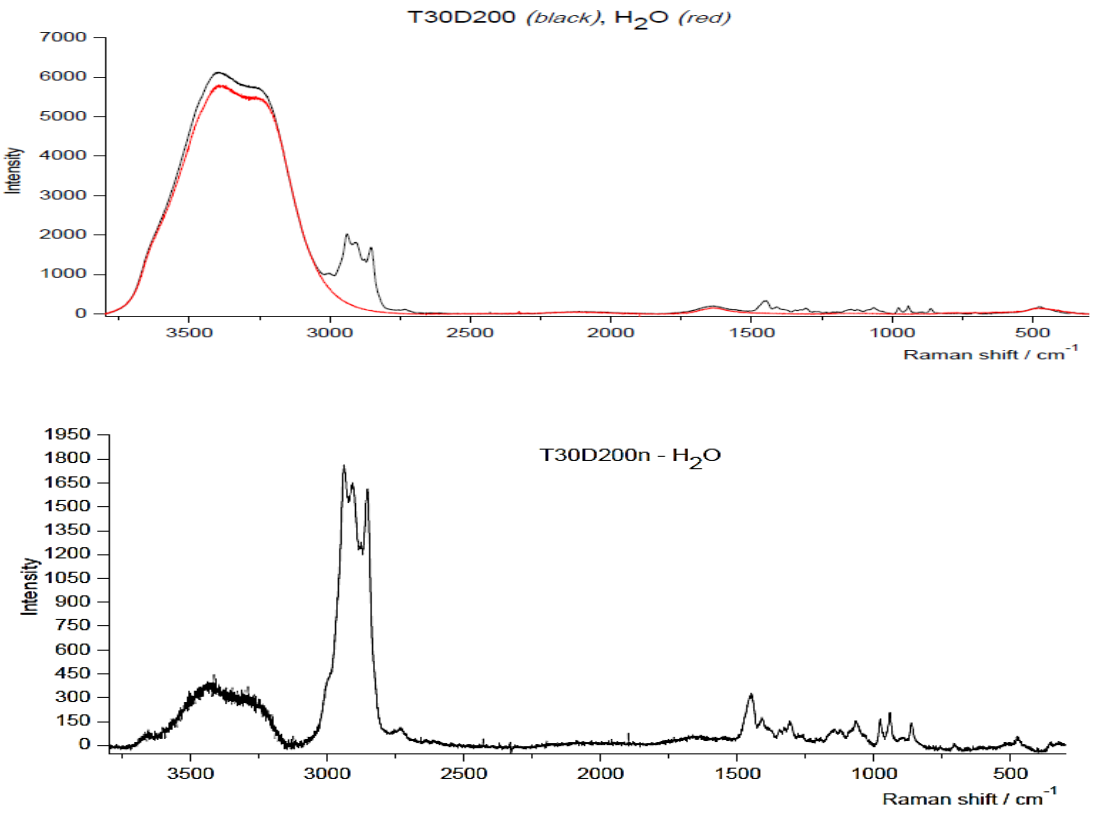

Figure 17. Normalization of the Raman spectrum of the aqueous solution T30D200 with the Raman OH stretching bands of Milli-Q water and the Raman spectrum resulting from the subsequent subtraction of the Raman spectrum of Milli-Q water (T30D200ns).

In order to subtract the spectrum corresponding to the excess of decanoate ion present in the T30D200 aqueous solution and obtain the interaction spectrum for the 1:1 inclusion complex ΔT30D200, we take the following spectral difference ΔT30D200=T30D200ns-(170/200)D200ns, as [TRIMEB_D]≈30 mM, [TRIMEB]≈0 and [D]≈170 mM.

Figure 18 shows the decomposition of the ΔB30D200 and ΔT30D200 Raman spectra in linear combinations of Lorentzian and Gaussian functions because the fact that CH stretching bands form a broad, structureless envelope, its necessary to decompose it to individual components. The decomposition of the ΔB30D200 Raman spectrum reveals bands with peak intensities at 2862 cm^{-1}, 2878 cm^{-1}, 2905 cm^{-1}, 2928 cm^{-1}, 2948 cm^{-1} and 2966 cm^{-1}, while the decomposition of the ΔT30D200 Raman spectrum exhibits peak intensities at 2825 cm^{-1}, 2848 cm^{-1}, 2880 cm^{-1}, 2905 cm^{-1}, 2944 cm^{-1} and 3000 cm^{-1}. These values are very similar to those in Figure 19 and they are in good agreement with the values in Table 1 and 2.

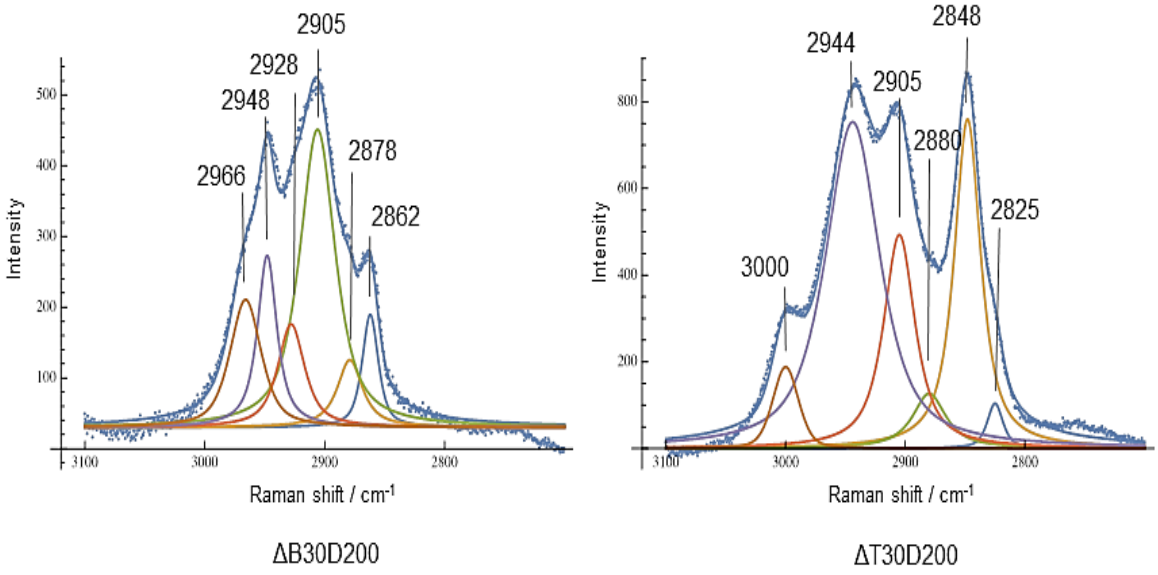

Figure 18. Decomposition in Lorentzian-Gaussian band profiles of the ΔB30D200 and ΔT30D200 Raman spectra in the Raman CH stretching wavenumber region.

Figure 19 shows the ΔT30D200, ΔT30D60 and ΔT30D200 - ΔT30D60 Raman spectra in the Raman CH stretching wavenumber between 2700 cm^{-1} and 3100 cm^{-1}. The latter spectrum takes the difference between the 1:1 inclusion complex Raman

spectra, above and below the decanoate ion CMC. In turn, Figure 20 shows the corresponding Raman spectra for the βCD aqueous solutions, namely, ΔB30D200, ΔB30D60 and ΔB30D200 - ΔB30D60 Raman spectra in the Raman CH stretching wavenumber, between 2700 cm^{-1} and 3100 cm^{-1}. While the ΔT30D200 - ΔT30D60 difference Raman spectrum indicates a significant increase of Raman intensities above the decanoate CMC, with respect to the corresponding Raman intensities below the sodium decanoate CMC (Figure 19), the ΔB30D200 - ΔB30D60 difference Raman spectrum shows less significant positive and negative intensity variations (Figure 20).

As you can see in the spectrum of ΔB30D60, below the CMC do not present intensity variations or significant frequency fluctuations. In turn, above the CMC, enhancements are observed in the region between 2700-3100 cm^{-1} (νCH). The wide band is registered with the intensity peak at 2940 cm^{-1}, which is caused by the valence vibrations of the stretching vibration of hydroxyl group bonded to C6-OH connected by the intermolecular hydrogen bonds or in the secondary hydroxyl groups connected by the intramolecular hydrogen bonds, the C2-OH group of one glucopyranose unit and C3-OH group of the adjacent glucopyranose unit). The other intensity peak at 2899 cm^{-1} is observed, belonging to the valence vibrations of the C-H bonds in the CH and CH_2 groups (Figure 20).

We can conclude, in general terms, the spectrum ΔB30D200 reveals βCD-micelle interactions of NaDec that are not confined to the simple inclusion of decanoate ion in cyclodextrin, suggesting an indirect interaction involving sodium decanoate micelles and βCD. If these interactions consisted only in the formation of inclusion complexes changes would be visible in the spectrum below the CMC (Figure 20).

The inclusion of ions of decanoate in βCD displaces the micelle-monomer equilibrium towards the monomer, reducing the aggregation number of micelles and yielding higher sizes of micelles dispersion. The OH stretching region is extremely complicated, because the primary and secondary OH groups of βCD may be bonded intra- or inter-molecularly, and hydrogen bonds may also be formed between the water molecules complexed in the cavity, or between the crystallization water molecules belonging to βCD [27].

These Raman spectroscopic findings remind us of the SANS results presented in [4] that clearly pointed to the adsorption of TRIMEB on the surface of the sodium decanoate micelles in contrast with βCD which was not adsorbed by these micelles.

Whereas $[NaDec]_0$ = 200 mM and CMC = 116 mM, the concentration of monomers in the micelles is equal to 84 mM. Using the aggregation number of micelles equal to 18.5 [4], then micelle concentration is approximately 4.5 mM. Assuming spherical micelles with a radius approximately equal to 15 Å and considering that the widest edge of TRIMEB corresponds to a circumference of radius approximately equal to 8 Å, then $[TRIMEB]_0$ = 30 mM corresponds to an approximately equal coverage to 50% of the micelles.

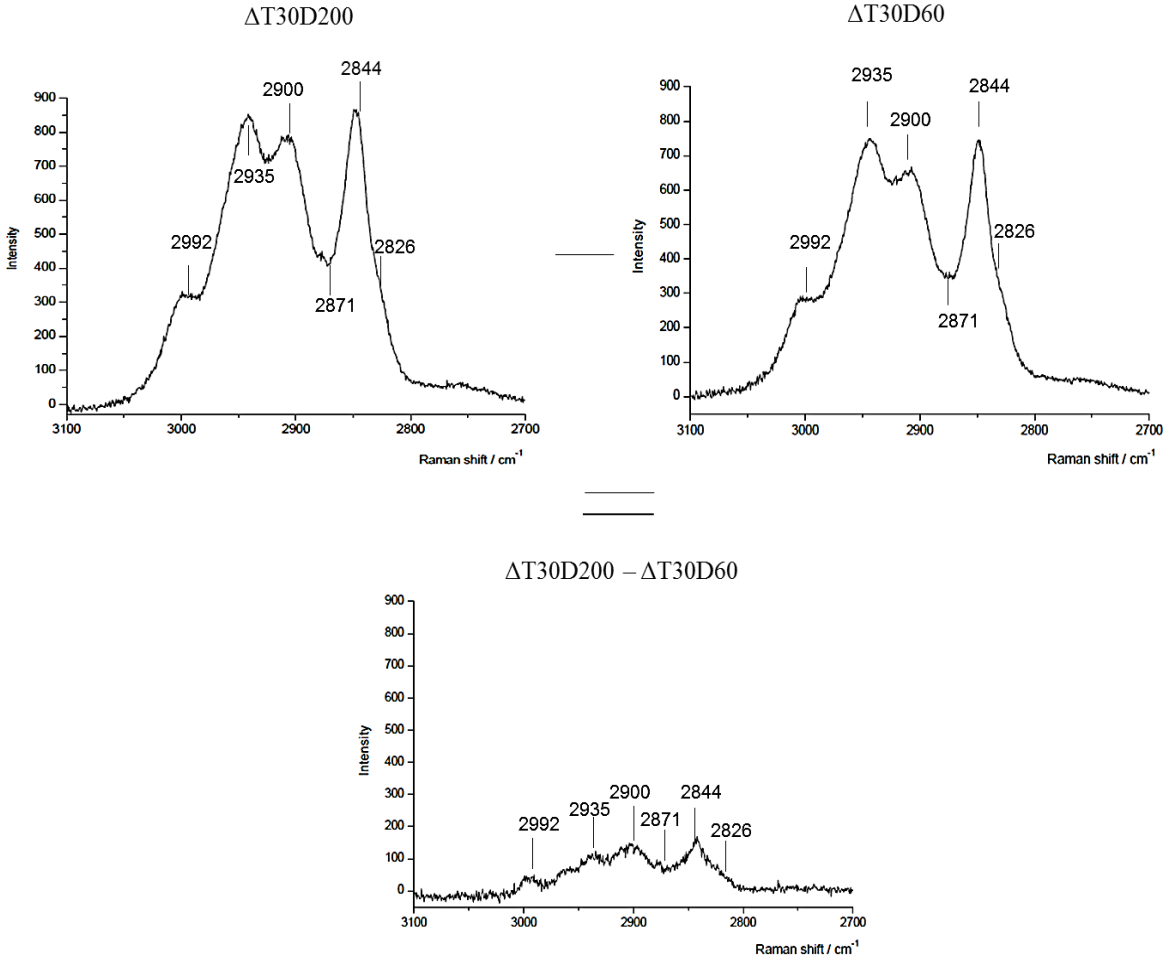

Figure 19. The Raman spectra ΔT30D200, ΔT30D60 and their difference ΔT30D200 - ΔT30D60 in the CH stretching region.

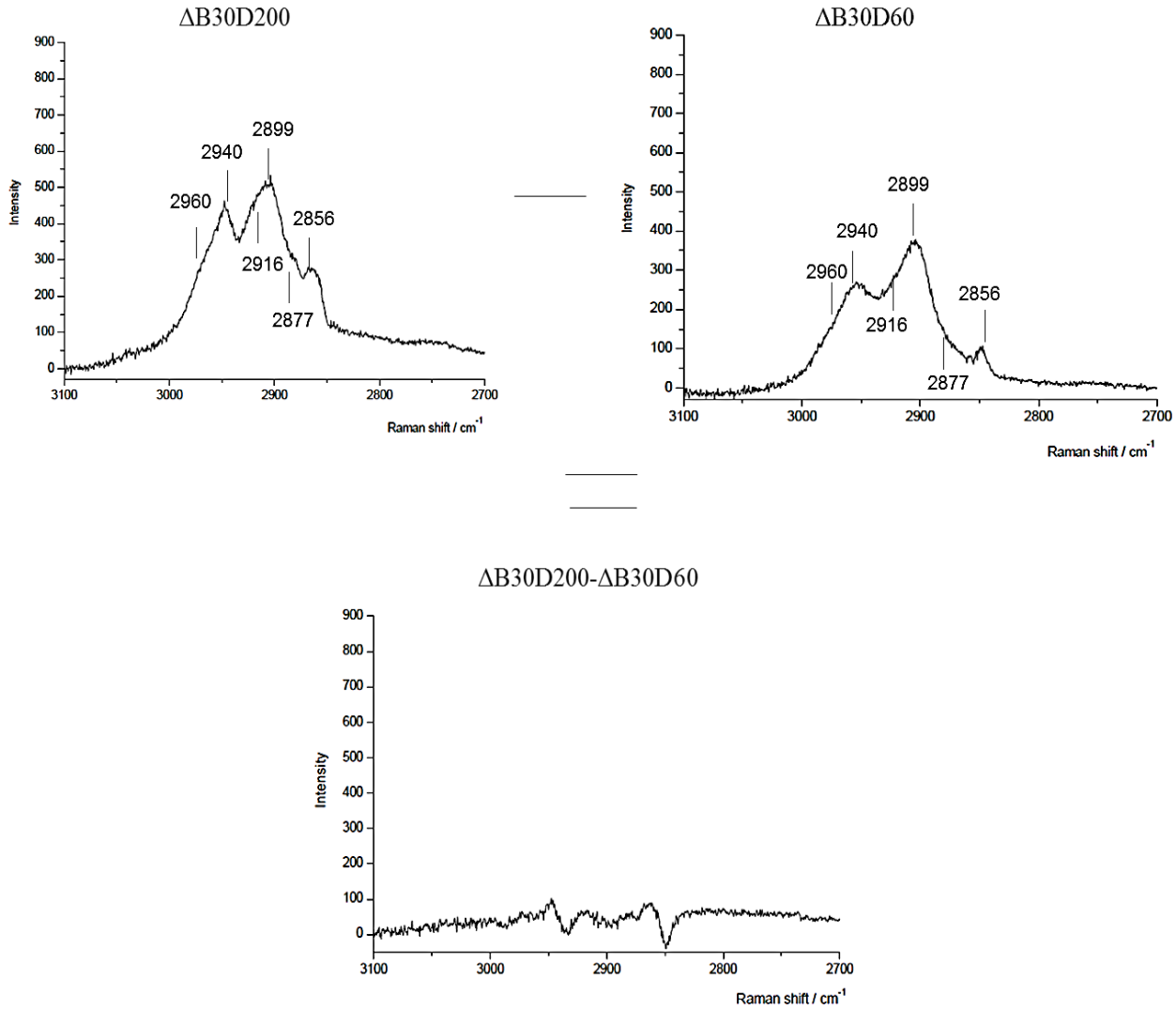

Figure 20. The Raman spectra ΔB30D200, ΔB30D60 and their difference ΔB30D200 - ΔB30D60 in the CH stretching region.

2 – SURFACE ENHANCED RAMAN SPECTRA FOR THE INTERACTION BETWEEN CYCLODEXTRINS AND *TRANS*–CINNAMIC ACID WITH SILVER NANOPARTICLES

2.1 - SERS SPECTRA OF *TRANS*–CINNAMIC ACID

The SERS spectrum of *t*-CIA was recorded on two different colloids and revealed different behaviors. The silver colloid borohydride shows a strong SERS spectrum, while the spectrum of silver colloid hydroxylamine present lower signal / noise ratio [21,44], giving these results we decided to work with silver colloid borohydride.

Figure 21 shows the spectrum of t-CIA and SERS spectrum of *t*-CIA in colloidal solution. The SERS spectrum is characterized by a set of strong and medium bands recorded at 1635 cm^{-1}, 1600 cm^{-1}, 1377 cm^{-1}, 1250 cm^{-1} and the band 1001 cm^{-1}. The band recorded at 1635 cm^{-1} assigned to ν(C=C) is characteristic of α, β-unsaturated carboxylic acids. The deviation of raman shift in the colloidal solution of the stretching vibration OCO at 1377 cm^{-1} compare to the spectrum of aqueous solution proves that the group acid interact with nanoparticles. The SERS band of *trans*-cinnamic acid assigned to vinyl vibrations at 1636 cm^{-1}, display a deviation of the raman frequency (Table 3), due to the fact that the band νOCO is bonded to the nanoparticles and the bands correspond to the aromatic ring 1601 cm^{-1}, 1253 cm-1 and 1002 cm-1 remain unperturbed in colloidal solution proving that this group is perpendicular to the surface of silver nanoparticles.

To observe the SERS effect is necessary to normalize the spectrum of *t*-CIA in aqueous solution with the spectrum of *t*-CIA in colloidal solution. We chose to work with the complex C=C stretching bands. Because its impossible to obtain a perfect match in all Raman shifts, preference is given to tmatch on the higher wavenumber wing of this complex of bands, so that stretching bands of benzene ring become free from overlapping. We represent Ag(colloidal)_*t*-CIAn for the spectrum after normalization and *n* stands for normalization (Figure 22).

SERS effect exhibit an intensification of Raman signal for *trans*-cinnamic acid adsorbed on silver nanoparticles. The Raman band of the acid adsorbed on silver surface is more intense than the acid in aqueous solution (Figure 22).

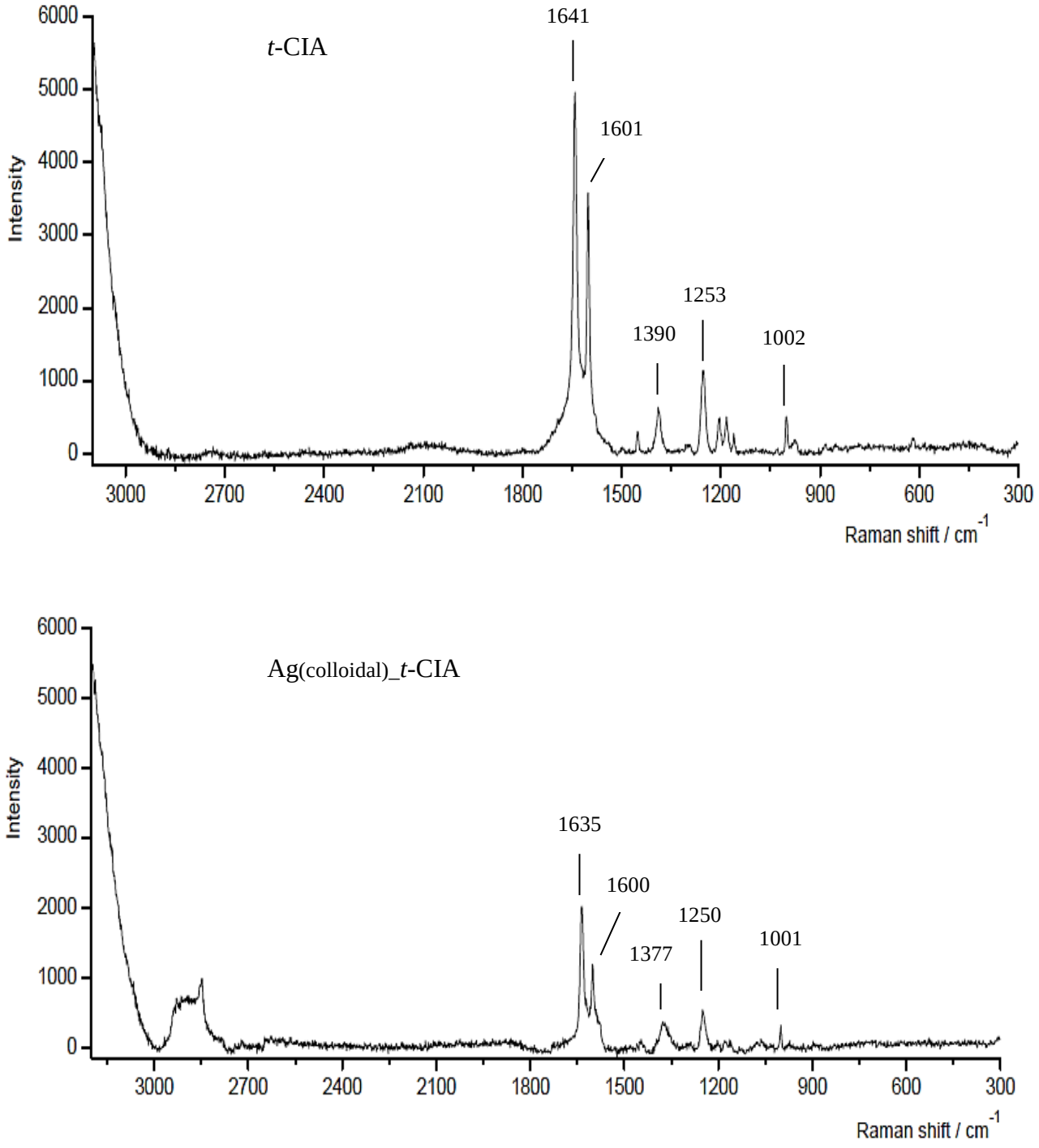

Figure 21. Raman spectrum of a 30 mM aqueous solution of sodium trans-cinnamate at pH 12 and SERS spectrum on silver colloid of a $3x10^{-4}$ M solution of *trans*-cinnamic acid.

t-CIA (*black*), Ag(colloidal)_*t*-CIAn *(red*)

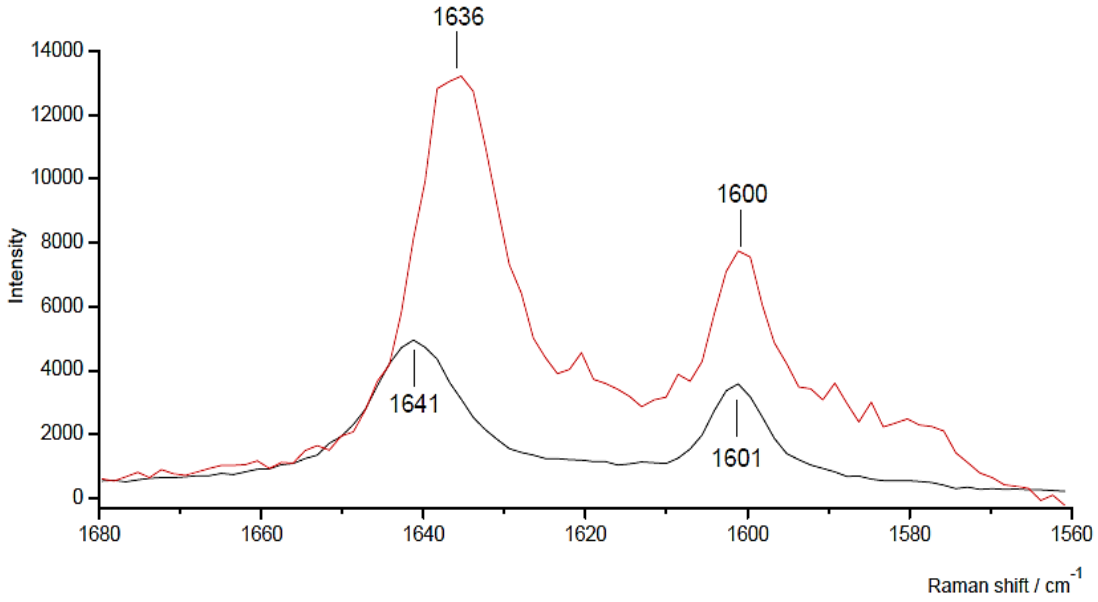

Figure 22. Normalization of SERS spectrum (red) of *trans*-cinnamic acid, Ag(colloidal)_*t*-CIAn, with Raman spectrum of sodium *trans*-cinnamate (black).

2.2 - INCLUSION COMPLEX 1:1 *TRANS*-CINNAMIC ACID AND TRIMETHYL-β-CYCLODEXTRIN

The inclusion of *trans*-cinnamic acid with methylate cyclodextrin is visible in the region of bands between 2700 and 3100 cm^{-1} (Figure 23), by means of the disappearance of aromatic *ν*C–H ring mode at 3074 cm^{-1} of *t*-CIA and presence of bands at 3000, 2946 and 2850 cm^{-1} corresponding to the stretching CHs vibration modes of TRIMEB. These frequencies are in accordance with the spectrum of methylate cyclodextrin in aqueous solution (Appendix 3) and proves that aromatic group of the acid is partially included within the cavity of the cyclodextrin.

The inclusion of *t*-CIA molecules display a *s-trans* orientation with CD molecules, stacked in a head-to-head arrangement. Because the carboxylate groups of *t*-CIA molecules are not close enough to form hydrogen-bonded dimers, carboxylate groups of *trans*-cinnamic molecules form O–H–O hydrogen bonds [56]. These

molecules have the propensity to bond with cyclodextrin cavities and lead to an elliptical distortion of the benzene ring.

A benzene structure measures approximately 7 x 7 x 3.4 Å and therefore is able to fit into the interior of the cyclodextrin cavity; also the side chain may fit into the cavity. With benzene ring diameter being roughly the same size as the cyclodextrin cavity a strong stability is expected, though strain is necessary due to the tight fit [40].

Stability constants for complexes composed of β-cyclodextrin and cinnamic acid are reported and ranged from 60 to 371 M^{-1}. The stability constant for the complex *t*-CIA_βCD formed at pH 1.6 and pH 8.2 is expected to be 371 to 313 M^{-1} [81]. Complexation between βCD and *trans*-cinnamic acid may be poor because the cavity size of βCD is too large to interact with the phenyl moiety of cinnamic acid. This theory is supported by a ^{13}C-nuclear magnetic resonance study [79]. For TRIMEB the value of constant stability isn't known, but we can assume that should be higher because the cavity is smaller than βCD and is partially obstructed with a methyl group, having a better inclusion with cinnamic acid, than βCD.

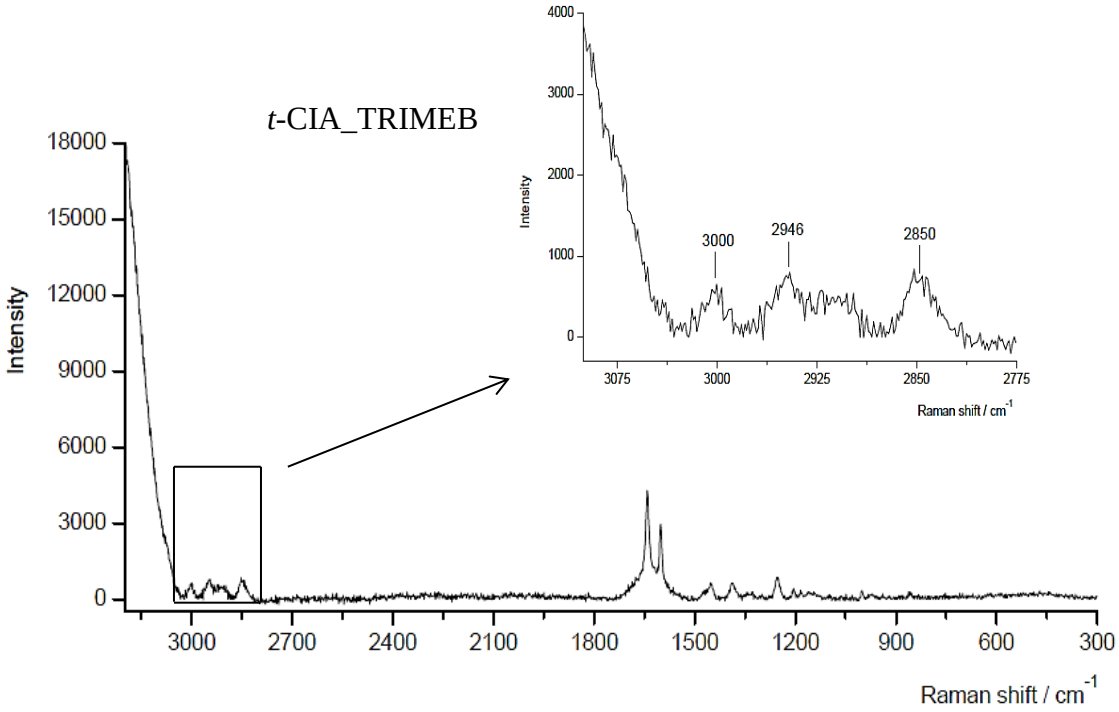

Figure 23. Raman spectrum of a 15 mM aqueous solution of the inclusion complex *trans*-cinnamate with trimethyl-β-cyclodextrin.

The presence of cyclodextrin in SERS wasn't visible (Figure 24), being the spectrum of Ag(colloidal)_*t*-CIA_TRIMEB very similar to that of Ag(colloidal) _*t*-CIA (Figure 21). In the spectrum of SERS is visible a band in the region between 2700-3100 cm^{-1} which is caused by the addition of sodium sulfate. Sodium sulfate act as a pre-aggregation agent, this aggregation allows a better SERS intensity, however it shouldn't appear any band on this region, the fact it appeared it can be due to impurities, sample preparation and others. This band will disguise the bands corresponding to the stretching vibration of CHs, the region which we know there's inclusion of cinnamic acid into the cyclodextrin.

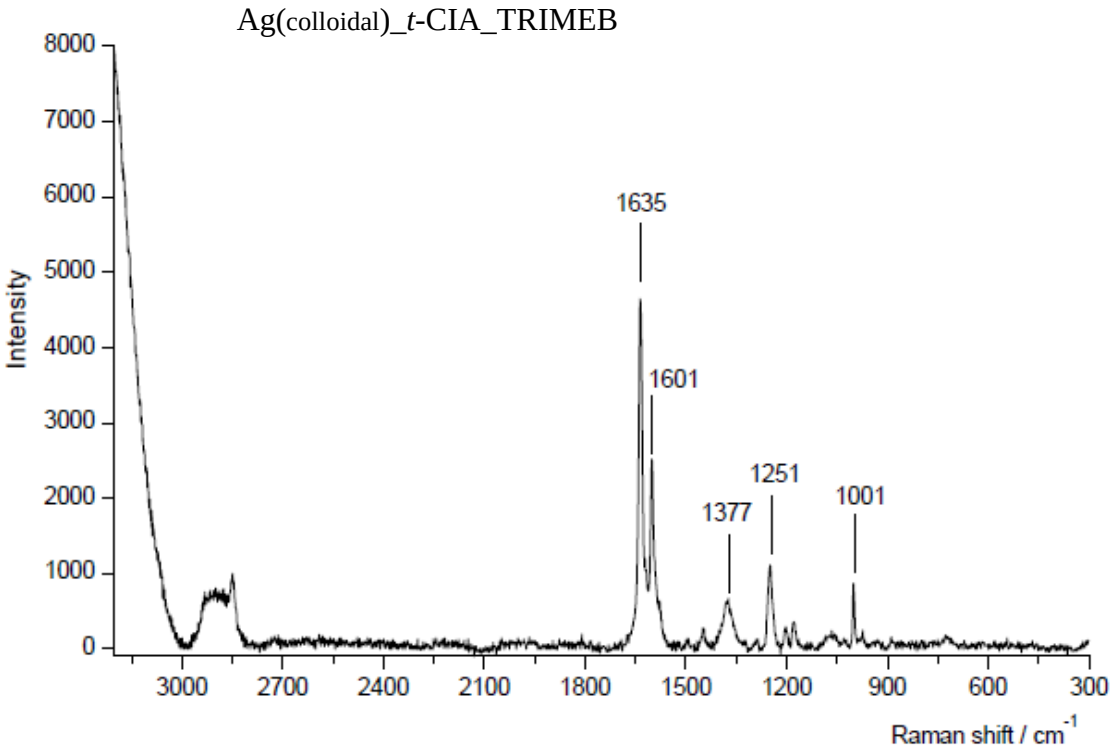

Figure 24. SERS spectrum of a $1.5x10^{-4}$ M aqueous solution of the inclusion complex *trans*-cinnamic acid with trimethyl-β-cyclodextrin. (colocar as frequencias das bandas)

2.3 – INTERACTION BETWEEN CYCLODEXTRINS AND SILVER NANOPARTICLES

Several attempts to observe SERS spectra from native and methylate cyclodextrins in colloidal solution yielded to negative results. Because we know there's inclusion of the acid into the cavity of cyclodextrin and the acid group interact with silver nanoparticles, in Figures 25 and 26 the region 1600-1640 cm^{-1} shows an increase of intensity, compare to the rest of the spectra, which we assume it's due to the presence of cyclodextrins.

The SERS intensities of the colloid borohydride were found to increase with time. The addition of one adsorbate as the cinnamic acid or this acid plus the cyclodextrin leads to an even higher intensity increase during a certain period of time. SERS intensities reach a maximum after a certain period of time and then decline in intensity due to flocculation of the colloid, this is the case of unsubstituted cyclodextrin. Although, the colloid is very stable for months its use is not convenient after several days, due to a change of chemical properties at the surface [60]. This instability is due to a lower electrostatic barrier that makes easier the approaching of different colloids to form aggregates and flocculate.

The intensity of *t*-CIA_βCD and *t*-CIA_TRIMEB in colloidal solution was evaluated during 1h30min. After 45 minutes, the intensity of Ag(colloidal)_*t*-CIA_βCD (Figure 25) reached its maximum, having a decay after 1hour whereas in Ag(colloidal)_*t*-CIA_TRIMEB the intensity reached its maximum after 1h30min (Figure 26). In colloidal solutions, is sometimes added an antiflocculant, for example, polyvinylpyrrolidone, to extend the life of the colloid [86]. TRIMEB delays the aggregation and the optimal size of aggregates appeared at longer times.

Methylate CDs stabilized colloidal solution and function as an antiflocculant, because they are weakly adsorbed on the metal surface [11] due to the presence of methyl groups in the narrow rim of the cyclodextrin. Both CDs affect the colloidal surface charge in different ways. This surface guarantees the stability of colloidal nanoparticles mostly due to repulsive Coulombic interactions [74].

The cavity of βCD is too small to entrap Ag_{np} and simply binds via chemisorption to silver nanoparticles through rim hydroxyl groups. This cavity can host single metallic cations or interact with the surface of silver nanoparticles depending on

size and shape. The edges of native cyclodextrin give rise to a local density in non-bonded electrons. This local electronic density is responsible for weak ion–dipole interactions with metallic ions and is responsible for the bonding of βCD to metallic surfaces [2].

On the whole, the absolute intensities in SERS were found to be somewhat irreproducible and so any conclusion concerning the comparison of absolute intensities between different cyclodextrins should require additional experiments.

Ag(colloidal)_*t*-CIA_βCD_45(*black*)_90(*red*)

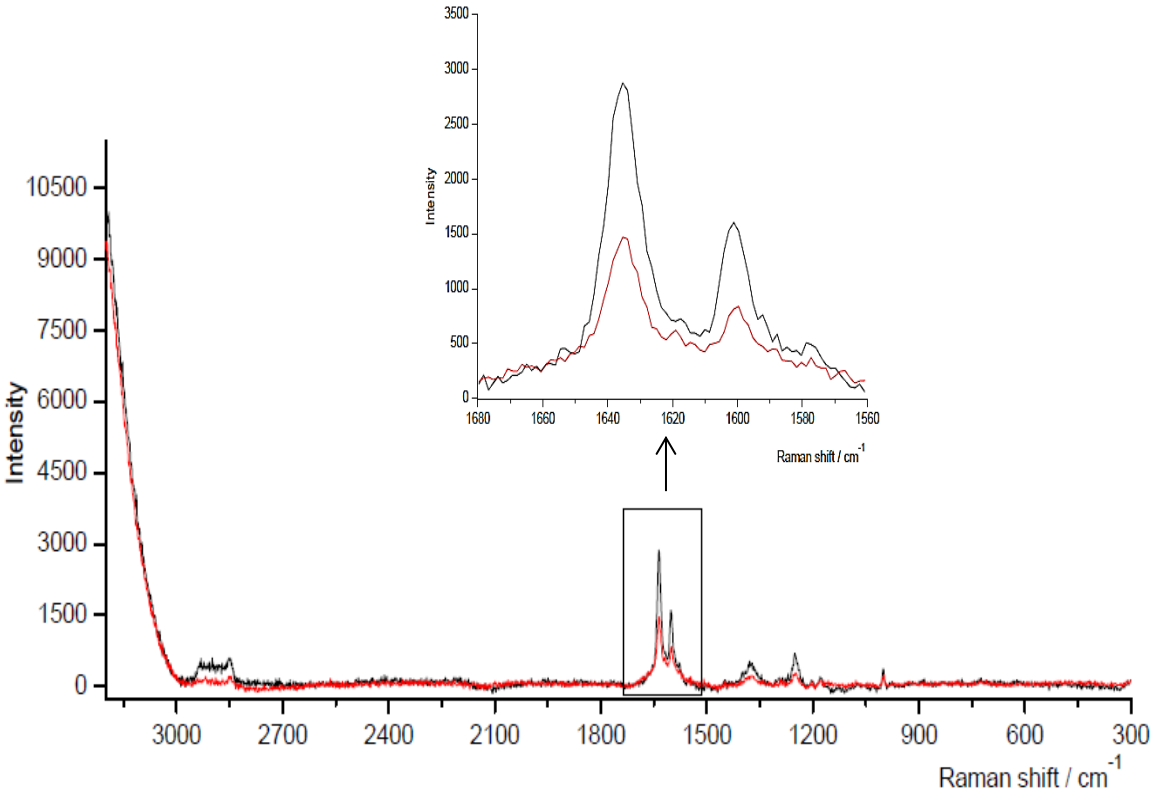

Figure 25. SERS spectra of a 1.5×10^{-4} M *trans*-cinnamic acid_ β-cyclodextrin at 45 minutes (black) and 90 minutes (red).

Ag(colloidal)_*t*-CIA_TRIMEB_45(*black*)_90(*red*)

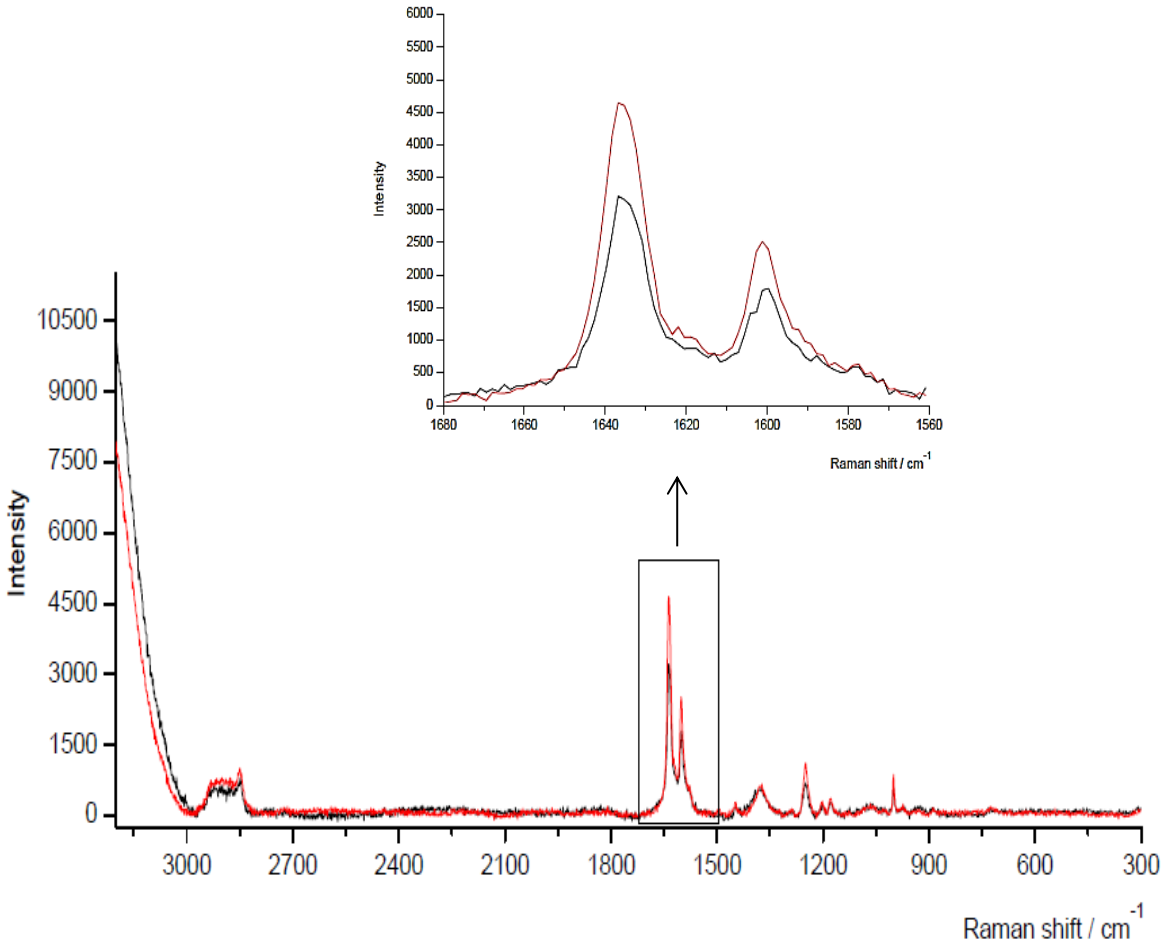

Figure 26. SERS spectra of a 1.5×10^{-4} M of *trans*-cinnamic acid_ trimethyl-β-cyclodextrin at 45 minutes (black) and 90 minutes (red).

Table 3. Experimental Raman and SERS vibrational wavenumbers (cm^{-1}) of *trans*-cinnamic acid and proposed assignment according to B3LYP/LanL2DZ theoretical calculation of different chemical species such as, *trans*-cinnamic acid (CIA), cinnamate (CIM^-) and the most stable superficial complex CIM^--Ag^+

Experimental Wavenumbers / cm^{-1}		**B3LYP/LanL2DZ Wavenumbers / cm^{-1}**			
Raman[a,b]	**SERS**[a,b]	**CIA**	**CIM^-**	**CIM^--Ag^+**	**Assignment**[c]
		3658			ν(O-H)
		3233	3215	3231	ν(C-H)
3074 (s)	3065 (vw)	3241	3161	3228	ν(C-H)e close to COO-
		3209	3205	3216	ν(C-H)
		3196	3192	3193	ν(C-H)
3031 (vw)		3191	3180	3188	ν(C-H)
1641 (vs)	**1635 (vs)**	**1699**	**1676**	**1689**	**ν (C=C)**
		1672	1571		ν(C-COO^-) + δ(COH)
1601 (vs)	**1600 (vs)**	**1650**	**1643**	**1651**	**8a; ν_{ring}**
		1623	1618	1625	8b; ν_{ring}
1500 (w)	1497 (vw)	1528	1519	1527	19a; ν_{ring}
				1425	$\nu_s(COO^-)$ + ν(C-H)e close to COO^-
1452 (w)	1448 (vw)	1482	1474	1480	19b; ν_{ring}
1390 (m)	1377 (m)	1393	1287	1391	$\nu_s(COO^-)$ + ν(C-H)e close to benzenic ring
1328 (vw)		1372	1317		δ(C-H) + δ(C-H)e (both)
1303 (w)		1337	1363	1373	δ(C-H) + δ(C-H)e close to benzenic ring
1294 (w)	1291 (w)	1272	1287	1336	δ(C-H)e close to COO^- + δ(COH)
		1272	1251	1277	δ(C-H)e close to COO^- + δ(COH)
1253 (s)	1250 (s)	1249	1251	1241	ν(C-X) + δ(C-H)e both
1205 (m)	1201 (w)	1225	1224	1222	δ(C-H) + ν(C-C)
1180 (m)	1179 (w)	1207	1210	1205	δ(C-H) + ν(C-C)
1162 (w)		1111	1196	1110	δ(C-H) + ν(C-C)
1030 (vw)	1029 (vw)	1025	1043	1053	γ(C-H) + γ(C-H)e both
1002 (m)	1001 (s)	1015	1012	1016	12; δ_{ring}
975 (w)	976 (w)	969	956	966	17a; γ(C-H) + γ(C-H)e both
880 (w)		883	874	881	γ(C-H)
855 (vw)		847	841	858	$\delta(COO^-)$ + 1; ν_{ring}
783 (vw)		726	799	804	$\gamma(C\text{-}H) + \gamma(CC)_{skeletal}$
	728	706	723	726	γ(C-H) + γ(C-H)e close to COO^-
		651	695	725	$\delta(C\text{-}C)_{skeletal}$
620 (w)		635	635	635	6a; δ_{ring}

[a]vs: very strong; s: strong; m: medium; w: weak; vw: very weak. [b]Aqueous solution of 30mM at pH=12. [c]Final concentration of the adsorbate $3x10^{-4}$ M at pH=12. [d]Wilson's Nomenclature. ν: stretching; δ: in-plane deformation; γ: out-of-plane deformation.

CONCLUSIONS

The intense complex of OH stretching bands of the water solvent usually dominates the Raman spectra of diluted aqueous solutions. An aqueous solution containing two weakly interacting solutes A and B yields a spectrum where it is difficult to identify frequency and Raman intensity variations due to the AB complex of weakly interacting solute molecules. Based on the integrated intensity of the complex of Raman OH stretching bands of liquid water as an external intensity standard, we use this band to obtain a difference spectrum that reveals Raman intensity changes mainly due the intermolecular interaction between the interacting solutes, provided one knows the equilibrium concentrations of A, B and AB species in aqueous solution. In addition, the method allows to qualitatively compare the different behaviours of TRIMEB and βCD in an aqueous solution of sodium decanoate above and below its CMC [4].

The study of the cyclodextrin-micelle interactions involving βCD and TRIMEB and sodium decanoate micelles in water shows predominant Raman band intensity changes in the CH stretching bands. In addition, qualitative differences in the interactions of βCD and TRIMEB with micelles of sodium decanoate in water have been observed, reflecting different modes of interaction of these cyclodextrins with the micelles. In particular, βCD indirectly interacts with the micelle displacing the monomer-micelle equilibrium towards the formation of monomer, thus causing a decrease in the number of aggregation and a decrease in the size of micelles.

On the other hand, TRIMEB is absorbed on the surfaces of the micelles, with roughly 50% of the surface of micelles being covered by TRIMEB molecules. In contrast to the behavior of βCD, the absorption of TRIMEB micelles minimizes the size of the micelles dispersion, the inclusion of decanoate ion in TRIMEB is only partial because this cyclodextrin has a central cavity partially obstructed by one of the methyl groups of the narrower cyclodextrin rim.

When in presence of silver nanoparticles, native cyclodextrins are adsorbed on the surface of silver colloidal particles via chemisorption through rim hydroxyl groups, stabilizing the colloidal solution during 45 minutes, whereas TRIMEB stabilizes the colloidal soltuion during 90 minutes. Methylate cyclodextrin act as a better surface stabilizer than βCD, improving the stability of colloidal solution and preventing aggregation.

Finally, we have been unable to obtain the ideal conditions in which a good comparison can be made between native and methylate cyclodextrins, using Surface Enhance Raman Spectroscopy. The absolute intensities in SERS were found to be somewhat irreproducible and so any conclusion concerning the comparison of absolute intensities between different cyclodextrins should require additional experiments.

Both cyclodextrins have different behaviours when in presence of colloidal particles. Methylate cyclodextrin is adsorbed on the surface of the sodium decanoate micelles in contrast with βCD which is not adsorbed by these micelles. In presence of silver nanoparticles natural cyclodextrin is adsorbed on the surface of silver colloidal particles while methylate cyclodextrin is not adsorbed.

REFERENCES

1. Ahmadi, T. S., Wang, Z. L., Green, T. C., Henglein, A. & El-Sayed, M. A. (1996). Shape-Controlled Synthesis of Colloidal Platinum Nanoparticles. *Science 272*, 1924-1926. **DOI**: 10.1126/science.272.5270.1924.

2. Amiri, S., Duroux, L. & Larsen, K. L. (2015). Silver nanoparticle colloids with γ-cyclodextrin: enhanced stability and Gibbs-Maragoni flow**.** *J. Nanopart Res*., 17, 17-21. **DOI**: 10.1007/s11051-014-2820-5.

3. Andrade-Dias, C., Lima S., Teixeira-Dias, J. J. C. & Teixeira, J. (2008). Why Do Methylated and Unsubstituted Cyclodextrins Interact So Differently with Sodium Decanoate Micelles in Water? *J. Phys. Chem. B*, 112, 15327–15332. **DOI**: 10.1021/jp807167h.

4. Andrade-Dias, C., Lima, S. & Teixeira-Dias, J. J. C. (2007). From simple amphiphilic to surfactant behavior: analysis of 1H NMR chemical shift variations. *J. Colloid Interface Sci***,** 316: 31-36. **DOI**: 10.1016/j.jcis.2007.07.049.

5. Arenas, J. F., Centeno, S. P., López-Tocón, I. & Otero, J. C**.** (2004). Surface-enhanced Raman scattering of 2,3-dimethylpyrazine adsorbed on silver electrode: selective enhancement explained through the charge transfer mechanism. *Vibrational Spectroscopy*, 35, 39–44. **DOI**: 10.1016/j.vibspec.2003.11.012.

6. Arenas, J. F., López-Tocón, I., Otero, J. C. & Marcos, J. I. (1999). The charge transfer mechanism in the SERS of 2-methylpyrazine on silver electrode. *Vibrational Spectroscopy*, 19, 213–221. **DOI**: 10.1016/S0924-2031(98)00095-2.

7. Arenas, J. F., Soto, J., López-Tocón, I., Fernández, D. J., Otero, J. & Marcos, J. I. (2002). The role of charge-transfer states of the metal-adsorbate complex in surface-enhanced Raman scattering**.** J. *Chem. Phys*., 116, 7207-7216. **DOI**: 10.1063/1.1450542.

8. Bender, M. L. & Komiyam, M. (1978). *Cyclodextrin Chemistry: Reactivity and Structure* – Berlin. Ed: Springer-Verlag Berlin Heidelberg. **DOI**: 10.1007/978-3-642-66842-5.

9. Braga, S. S., Aree, T., Imamura K., Vertut, P., Boal-Palheiros, I., Saenger, W. & Teixeira-Dias, J. J. C (2002). Structure of the β-Cyclodextrin.*p*-Hydroxybenzaldehyde Inclusion Complex in Aqueous Solution and in the Crystalline State. *J. Inclusion Phenom. Macro. Chem***,** 43, 115-125. **DOI**: 10.1023/A:1020412412907.

10. Braga, S. S., Gonçalves, I. S., Herdtweck, E. & Teixeira-Dias, J. J. C. (2003). Solid state inclusion compound of S-ibuprofen in β-cyclodextrin: structure and characterization. *New J. Chem*, 27, 597-601. **DOI**: 10.1039/b207272f.

11. Bricout, H., Hapiot, F., Ponchel, A., Tilloy, S. & Monflier, E. (2009). Chemically Modified Cyclodextrins: An Attractive Class of Supramolecular Hosts for the Development of Aqueous Biphasic Catalytic Processes. *Sustainability***.** 1, 924-945. **DOI**: 10.3390/su1040924.

12. Burkitt, S. J., Ottewill, R. H., Hayter, J. B. & Ingram B. T. (1987). Small angle neutron scattering studies on micellar systems Part 1. Ammonium octanoate, ammonium decanoate and ammonium perfluoroocatanoate. *Colloid Polym. Sci*, 265, 619–627. **DOI**: 10.1007/BF01412778.

13. Campion, A. & Kambhapati, P. (1998). Surface-enhanced Raman scattering - *Chemical Society Reviews*, 27: 241-250. **DOI**: 10.1039/A827241Z

14. Carey, D. M. & Korenowski, G. M. (1998). Measurement of the Raman Spectrum of liquid water. *J. Chem. Phys.*, 108, 2669-2675. **DOI**: 10.1063/1.475659.

15. Castro, J. L., López, R. M. R., López, T. I. & Otero, J. C. (2002). Surface – enhanced Raman scattering of 3-phenylpropionic acid (hydrocinnamic acid). *J. T. Spec*, 33, 455-459. **DOI**: 10.1002/jrs.853.

16. Chambel, A., Viegas, C. A. & Sá-Correia, I. (1999). Effect of cinnamic acid on the growth and on plasma membrane H^+-ATPase activity of Saccharomyces cerevisiae. *International Journal of Food Microbiology*, 50, 173-179. **DOI**: 10.1016/S0168-1605(99)00100-2.

17. Clapperton, R. M., Ottewill, R. H., Rennie, A. R. & Ingram B. T. (1999). Comparison of the size and shape of ammonium decanoate and ammonium dodecanoate micelles. *Colloid Polym. Sci,* 277, 15–24. DOI: 10.1007/s003960050362.

18. Connors, K. & Rosanske, T. W. (1980). *trans*-Cinnamic Acid-α-cyclodextrin system as studied by solubility, spectral, and potentiometric techniques. *J. of Pharmaceutical Sciences***,** 69,173-179. **DOI**: 10.1002/jps.2600690215.

19. Connors, K. A. (1997). The Stability of Cyclodextrin Complexes in Solution. *Chem. Rev*., 97, 1325-1357. **DOI**: 10.1021/cr960371r.

20. Creighton, J. A. (1998). The Selection Rules for Surface-Enhanced Raman Spectroscopy. In Clark, R. J. H. & Hester, R. E. (1998). *Spectroscopy of Surfaces. Advances in Spectroscopy***.** New York: John Wiley & Sons Inc, 26 37-89.

21. Creighton, J. A., Blatchford, C. G. & Albrecht, M. G. (1979). Plasma resonance enhancement of Raman scattering by pyridine adsorbed on silver or gold sol particles of size comparable to the excitation wavelength. *J. Chem. Soc. Faraday Trans*., 75, 790-798. **DOI**: 10.1039/F29797500790.

22. Cristiano, A. D., Sérgio, L. & Teixeira-Dias, J. J. C. (2007). From simple amphiphilic to surfactant behavior: Analysis of ^{1}H NMR chemical shift variations. *J. Colloid Interface Sci.***,** 316, 31–36. **DOI**: 10.1016/j.jcis.2007.07.049.

23. Davidson, M., Sofos, J. & Branen, A. L (2005). *Antimicrobials in Food.* London: Taylor and Francis, 3ed.

24. Del Valle, E. M. M. (2003). Cyclodextrins and their uses: a review. *Process Biochemistry***. DOI**: 10.1016/S0032-9592(03)00258-9.

25. DiLella, D. P., Gohin, A., Lipson, R. H., McBreen, P. & Moskovits, M. (1980). Surface-enhanced Raman spectroscopy of benzene and benzene-d_6 adsorbed on silver. *J. Chem. Phys.*, 73, 4282. **DOI**: 10.1063/1.440142.

26. Eastburn, S. D. & Tao, B. Y. (1994). Applications of modified cyclodextrins. *Biotechnol Adv.*, 12, 325–339. **DOI**: 10.1016/0734-9750(94)90015-9.

27. Egyed, O. (1990). Spectroscopic studies on β-cyclodextrin. *V. Spectroscopy***,** 1, 225-227. **DOI**: 10.1016/0924-2031(90)80041-2.

28. Eom, S. Y., Ryu, S. L., Kim, H. L. & Kwon, C. H. (2013). Systematic preparation of colloidal silver nanoparticles for effective SERS Substrates. *Colloids and Surfaces A: Physicochem. Eng. Aspects***,** 422, 39–43. **DOI**: 10.1016/j.colsurfa.2013.01.036.

29. Ferraro, J. R., Nakamoto, K. & Brown, C. W. (2003). *Introductory Raman Spectroscopy*. U.S: Academic Press, 2 ª ed.

30. Fleischmann, M., Hendra, P. J. & McQuillam, A. J. (1974). Raman spectra of pyridine adsorbed at a silver electrode. *Chemical Physics Letters*, 26, 163–166. **DOI**: 10.1016/0009-2614(74)85388-1.

31. Frisch, M. J., Trucks, G. W., Schlegel, H. B., Scuseria, G. E., Robb M. A., Cheeseman, J. R., Scalmani, G.,… Fox D. J. (2009). *Gaussian 09, Revision A.1* - Gaussian Inc: Wallingford C.T.

32. Fryling, M., Frank, C. J. & McCreery, R. L. (1993). Intensity calibration and sensitivity comparisons for CCD/Raman spectrometers. *Appl. Spectrosc*, 47, 1965-1974. **DOI**: 10.1366/0003702934066226.

33. Funasaki, N., Yodo, H., Hada, S. & Neya, S. (1992). Stoichiometries and Equilibrium-Constants of Cyclodextrin - Surfactant Complexations. *Bull. Chem. Soc*, 65, 1323-1330. **DOI**: 10.1246/bcsj.65.1323.

34. Haynes, W. M., Lide, D. R. & Bruno, T. J. (2015). *CRC Handbook of Chemistry and Physics*. London: CRC Press, Taylor and Frances Group, 96th Edition.

35. Hecht, E. (2002). *Optics*. California: Addison-Wesley, 4ª ed.

36. Hoff, C. A. (2013). *Correlation of Surface Enhanced Raman Spectroscopy and Nanoparticle Aggregation with Rhodamine 6G* - Master's Theses paper 4390. San José State University. Acedido 13-10-2015. Disponível em http://scaolarworks.sjsu.edu/edd_theses.

37. Iliescu, T., Baia, M. & Maniu, D. (2008). Raman and Surface Enhanced Raman Spectroscopy on molecules of Pharmaceutical and Biological interest**.** *Romanian Reports in Physics*, 60, 829–855. **DOI**: 10.1007/978-3-540-78283-4.

38. Jeanmaire, D. L. & Van Duyne, R. P. (1977). Surface raman spectroelectrochemistry: Part I. Heterocyclic, aromatic, and aliphatic amines adsorbed on the anodized silver electrode. J. *of Electroanalytical Chemistry and Interfacial Electrochemistry,* 84, 1-20. **DOI**: 10.1016/S0022-0728(77)80224-6.

39. Kusmin, A., Lechner, R. E., Kammel, M. & Saenger, W. (2008). Native and Methylated Cyclodextrins with Positive and Negative Solubility Coefficients in Water Studied by SAXS and SANS**.** *J. Phys. Chem. B.*, 112, 12888–12898. **DOI**: 10.1021/jp802031w.

40. Lach, J. L. & Cohen, J. (1963). Interaction of Pharmaceuticals with Schardinger dextrins. II. Interaction with selected compounds. *J. Pham. Sci*., 52, 137-142. **DOI**: 10.1002/jps.2600520207.

41. Laor, U. & Schatz, G.C. (1981). The Role of Surface Roughness in Surface Enhanced Raman Spectroscopy (SERS): The Importance of Multiple Plasmon Resonances. *Chem. Phys. Lett***.,** 82, 566-570. **DOI**: 10.1016/0009-2614(81)85442-5.

42. LaPlante, S., Halaciuga, I. & Goia, D.V. (2011). Preparation of counterion stabilized concentrated silver sols. *J. Colloid Interface Sci*., 359, 121-125. **DOI**: 10.1016/j.jcis.2011.03.080.

43. Lee, P. C. & Meisel, D. (1982). Adsorption and surface-enhanced Raman of dyes on silver and gold sols. *J. Phys. Chem*., 86, 3991-3395. **DOI**: 10.1021/j100214a025.

44. Leopold, N. & Lendle, B. (2003). A New Method for Fast Preparation of Highly Surface-Enhanced Raman Scattering (SERS) Active Silver Colloids at Room Temperature by Reduction of Silver Nitrate with Hydroxylamine Hydrochloride. *J. Phys. Chem. B.*, 107, 5723-5727. **DOI**: 10.1021/jp027460u.

45. Long, D. A. (2002). *The Raman effect: a unified treatment of the theory of Raman scattering by molecules*. New York: Ed. John Wiley and Sons Inc.

46. Machado, N. F. L., Ruano, C., Castro, J. L., Marquesa, M. P. M. & Otero, J. C. (2011). Chromone-3-carboxylic acid as a potential electron scavenger: a surface-enhanced Raman scattering study**.** *Phys. Chem. Chem. Phys*., 13, 1012–1018. **DOI**: 10.1039/c0cp01174f.

47. McCreery, R (2002). *Handbook of Vibrational Spectroscopy*. London: John Wiley & Sons Ltd. **DOI:** 10.1002/0470027320.s0706.

48. Moore, B. C. (1979). *Chemical and Biochemical Applications of Lasers*. New York: Academic Press. vol. 4.

49. Morigaki, K., Walde, P., Misran, M. & Robinson, B. H. (2003). Thermodynamic and kinetic stability. Properties of micelles and vesicles formed by the decanoic acid/decanoate system. *Colloids and Surfaces A: Physicochem. Eng. Aspects*, 213, 37-44. **DOI**: 10.1016/S0927-7757(02)00336-9.

50. Morton, S. M., Silverstein, D. W. & Jensen, L. (2011). Theoretical Studies of Plasmonics using Electronic Structure Methods. *Chemical Reviews*, 111, 3962–3994. **DOI**: 10.1021/cr100265f.

51. Moskovits, M. & Suh, J. S. (1985). Conformation of mono- and dicarboxylic acids adsorbed on silver surfaces. *J. Am. Chem. Soc***.,** 107, 6826-6829. **DOI**: 10.1021/ja00310a014.

52. Moskovits, M., DiLella, D. P. & Maynard, K. J. (1988). Surface Raman spectroscopy of a number of cyclic aromatic molecules adsorbed on silver: selection rules and molecular reorientation. *Langmuir*, 4, 67–76. **DOI**: 10.1021/la00079a012.

53. Mukerjee, P. & Mysels, K. J. (1971). *Critical Micelle Concentrations of Aqueous Surfactant Systems.* Washington: DC: NSRDS-NBS 36.

54. Muskens, O., Christofilos, D., Fatti, N. D. & Vallée, F. (2006). Optical response of a single noble metal nanoparticle. *J. of Opt A: Pure and Appl. Opt***.,** 8, 264–272. **DOI**: 10.1088/1464-4258/8/4/S28.

55. National Institute of Standards and Technology (2015). *Computational Chemistry Comparison and Benchmark Database. NIST Standard Reference.* Acedido 14-11-2015. Disponível em http://cccbdb.nist.gov/.

56. Nolasco, M. M., Amado, A. N. & Ribeiro-Claro, P. J. A. (2009). Spetroscopic and thermal studies on the inclusion of trans-cinnamic acid and a number of its hydroxyl-derivatives with α, β and γ-cyclodextrins molecules. *J. Raman Spect***.**, 40, 687-695. **DOI**: 10.1002/jrs.2182.

57. Otto, A., Timper, J., Billmann, J., Kovacs, G. & Pockrand, I. (1980). Surface roughness induced electronic Raman scattering. *Surf. Sci*., 92. 55-57. **DOI**: 10.1016/0039-6028(80)90237-X.

58. Pakoulev, A., Pang, Y., Dlott, D. D. & Wang, Z. (2004). Vibration substructure in the OH stretching transition of water and HOD. *J. Phys. Chem*, 108, 9054-9063. **DOI**: 10.1021/jp048545t.

59. Parker, K. M. & Stalcup, A. M. (2008). Affinity capillary electrophoresis and isothermal titration calorimetry for the determination of fatty acid binding with β-cyclodextrin. *J. Chromatography***,** 1204, 171-182. **DOI**: 10.1016/j.chroma.2008.02.050.

60. Pinto, V. V., Ferreira, M. J., Silva, R., Santos, H. A., Silva, F. & Pereira, C. M. (2010). Long-time effect on the stability of silver nanoparticles in aqueous medium: Effect of the synthesis and storage conditions. *Colloids and Surfaces A: Physicochem. Eng. Aspects.* 364. 19–25. **DOI**: 10.1016/j.colsurfa.2010.04.015.

61. Rahman, M. M., Khan, S B., Jamal, A., Faisal M. & Aisiri A. M. (2011). Iron Oxide Nanoparticles. In Rahman, M. M. (2011) *Nanotechnology and Nanomaterials.* Najran Kingdom of Saudi Arabia, 3, 43-66. **DOI:** 10.5772/27698

62. Ribeiro-Claro, P. J. A., Amorim, da Costa A. M., Vueba, M. L., Pina, M. E. & Amado A. M. (2006). *para*-Halogenated Benzaldehyde Molecules Included in Cyclodextrins: A Combined Spectroscopic and Thermal Analysis. *J. Raman Spectrosc.*, 37, 472-479. **DOI**: 10.1002/jrs.1419.

63. Richard, J. F. (2006). *Chemistry and Technology of Surfactants*. Oxford: UK. Blackwell Publishing Ltd.

64. Rivas, L., Sanchez-Cortez, S., Garcia-Ramos, J. V. & Marcillo, G. (2001). Growth of Silver colloidal Particles Obtained by Citrate Reduction to Increase the Raman Enhancement Factor. *Langmuir*, 17, 574. **DOI**: 10.1021/la001038s.

65. Saenger, W. R., Jacob, J., Gessler, K., Steiner, T., Hoffmann, D., Sanbe, H.,… Takaha, T. (1998). Structures of the Common Cyclodextrins and their Larger Analogues - Beyond the Doughnut**.** *Chem. Rev*., 98, 1787-1802. **DOI**: 10.1021/cr9700181.

66. Schatz, G. C. & Van Duyne, R. P. (2002). Electromagnetic Mechanism of Surface-enhanced Spectroscopy**.** In Chalmers, J. M. & Griffiths, P. R. (2002). *Handbook of Vibrational Spectroscopy*. London: John Wiley & Sons Ltd. **DOI**: 10.1002/0470027320.s0601.

67. Schneiderman, E. & Stalcup, A. M. (2000). Cyclodextrins: a versatile tool in separation science. *J. Chromatogr B*, 745, 83–102. **DOI**: 10.1016/S0378-4347(00)00057-8.

68. Sharma, B., Frontiera, R. R., Henry, A., Ringe, E. & Van Duyne, R. P. (2012). SERS: Materials, applications and the future**.** *MaterialsToday***,** 15, 16–25. **DOI**: 10.1016/S1369-7021(12)70017-2.

69. Siddhanta, S., Narayana C. (2012). Surface Enhanced Raman Spectroscopy of Proteins: Implications for Drug Designing. *Nanomater Nanotechnol*, 2, 1. **DOI**: 10.5772/46209

70. Skoog, D., Holler, F. & Crouch, S. (2007). *Principles of Instrumental Analysis*. Philadelphia: Thomson brooks/Cole, 6th ed.

71. Stiufiuc, R., Iacovita, C., Lucaciu, C. M., Stiufiuc, G., Dutu, A. G., Braescu, C. & Leopold, N. (2013). SERS-active silver colloids prepared by reduction of silver nitrate with short-chain polyethylene glycol. *Nanoscale Research Letter,* 8, 47. **DOI:** 10.1186/1556-276X-8-47.

72. Sun, Q. & Qin, C. (2011). Raman OH stretching band of water as an internal standard to determinate carbonate concentrations. *Chem. Geology*, 283. 274–278. **DOI**: 10.1016/j.chemgeo.2011.01.025.

73. Sun, Q. (2009). The Raman OH stretching bands of liquid water. *Vib. Spectrosc.***,** 51, 213-217. DOI: 10.1016/j.vibspec.2009.05.002.

74. Sylvestre, J. P., Kabashin, A. V., Sacher, E., Meunier, M. & Luong, J. H. T**.** (2004). Stabilization and size control of gold nanoparticles during laser ablation in aqueous cyclodextrins. *J. Am. Chem. Soc***.,** 126, 7176-7177. **DOI**: 10.1021/ja048678s.

75. Szejtli, J. (1996). Inclusion of guest molecules, selectivity and molecular recognition by cyclodextrins. In Szetjli, J. & Osa, T. (1996). *Comprehensive Supramolecular Chemistry***.** Oxford: Eds Pergamon, vol. 3, 189-203.

76. Szejtli, J. (1998). Introduction and General Overview of Cyclodextrin Chemistry. *Chem. Rev*., 98, 1743-1753. **DOI**: 10.1021/cr970022c.

77. Szymanski H. A. (1967). *Raman Spectroscopy, Theory and Practice*. U.S: Springer, 1ª ed. **DOI**: 10.1007/978-1-4684-3027-1.

78. Teschke, O., Ceotto, G. & Souza, E. F. (2001). Interfacial water dielectric-permittivity-profile measurements using atomic force microscopy. *Phys Rev. E.* 64011605; DOI: 10.1103.

79. Uekama, K., Hirayama, F., Esaki, K. & Inoue, M. (1979). Inclusion complexes of Cyclodextrins with Cinnamic Acid Derivatives: Dissolution and Thermal Behaviour. *Chem. Pharm. Bull*, 27, 76-79. **DOI**: 10.1248/cpb.27.76.

80. Uekama, K., Irie, T. & Duchene, D. (1987). Pharmaceutical Applications of Methylated Cyclodextrin Derivatives. In: Duchene, D. (1987). *Cyclodextrins and Their Industrial Uses.* Paris: Editions de Santé, 395-439.

81. Uekama, K., Otagiri, M., Kanie, Y., Tanaka, S. & Ikeda K**.** (1975). Inclusion Complexes of Cinnamic Acids with Cyclodextrins. Mode of Inclusion in Aqueous Solution. *Chem. Pharm. Bull*, 23, 1421-1430. **DOI**: 10.1248/cpb.23.1421.

82. Villiers, A. (1891). Sur la fermentation de la fécule par l'action du ferment butyrique. *Compt Rend. Acad. Sci*, 112, 536 – 538. Acessível na Biblioteca do Departamento de Química da Universidade de Coimbra, Portugal.

83. Walrafen, G. E., Fisher, M. R., Hokmabadi, M. S. & Yang, W. H. (1986). Temperature dependence of the low- and high-frequency Raman scattering from liquid water. *J. Chem. Phys*., 85, 6970-6982. **DOI**: 10.1063/1.451384.

84. Wan, Q., Spanu, L., Galli, G. A. & Gygi, F. (2013). Raman spectra of liquid water from ab initio molecular dynamics: vibrational signatures of charge fluctuations in the hydrogen bond network. *J. Chem. Theory Comput*., 9, 4124–4130. **DOI**: 10.1021/ct4005307.

85. Wenz, G. (2012). Influence of intramolecular hydrogen bonds on the binding potential of methylated β-cyclodextrin derivatives. *Beilstein J. Org. Chem*., 8, 1890–1895**. DOI**: 10.3762/bjoc.8.218.

86. Widoniak, J., Eiden-Assmann, S. & Maret, G. (2005). Silver particles tailoring of shapes and sizes. *Colloid Surf.*, 270/271, 340–344. **DOI**: 10.1016/j.colsurfa.2005.09.004.

87. Wolfram Research (2010). **Mathematic®.** Version 10.2.0.0, Platform Mac OSX, Inc. Champaign, Illinois, C.D.

88. Zabel, V., Saenger, W. & Mason, S. A. (1986). Neutron diffraction study of the hydrogen bonding in β-cyclodextrin undecahydrate at 120 K: from dynamic flip-flops to static homodromic chains. *J. Am. Soc***.,** 108, 3664-3673. **DOI**: 10.1021/ja00273a020.

ANNEX

A
N
N
E
X
1

Erasmus Internship acceptance Letter from Professor Juan Carlos Molina at University of Malaga

UNIVERSIDAD DE MÁLAGA

Dr. Juan Carlos Otero Fernández de Molina
Departamento de Química Física
Facultad de Ciencias
Universidad de Málaga
Campus de Teatinos s/n
29071-Málaga

Málaga, 24 de octubre de 2014

Juan Carlos Otero Fdez. de Molina, Catedrático de Universidad y Director del Departamento de Química Física de la Universidad de Málaga (UMA), hace constar que este Departamento acepta a la alumna de Maestrado Ana Filipa Santos Seiça, para una estancia de prácticas dentro del programa ERASMUS.

Esta estancia será por un periodo de seis meses, desde octubre de 2015 hasta marzo de 2016, para realizar experimentos Raman y SERS de derivados de ácidos orgánicos saturados y aromáticos, que complementarán a las tareas realizadas en la Universidad de Coimbra para el completar el proyecto de maestrado. Toda la actividad de la alumna será objeto de seguimiento continuo por mi parte, de manera que cada dos semanas se realizará una valoración del trabajo realizado en ese periodo, así como al final de la estancia, en donde se validará la consecución de los objetivos previstos.

El departamento de la UMA pondrá a disposición de la alumna los medios materiales necesarios para la tareas previstas.

Fdo. Juan C. Otero
Director del Departamento

A
N
N
E
X
2

Raman Spectroscopic evidence for the inclusion of decanoate ion in trimethyl-β-cyclodextrin

Vibrational Spectroscopy 85 (2016) 175–180

Contents lists available at ScienceDirect

Vibrational Spectroscopy

journal homepage: www.elsevier.com/locate/vibspec

Raman spectroscopic evidence for the inclusion of decanoate ion in trimethyl-β-cyclodextrin

Ana Filipa Seiça, Luís A.E. Batista de Carvalho, M. Paula M. Marques, José J.C. Teixeira Dias*

Research & Development Unit "Química-Física Molecular", University of Coimbra, 3004-535 Coimbra, Portugal

ARTICLE INFO

Article history:
Received 1 February 2016
Received in revised form 20 April 2016
Accepted 20 April 2016
Available online 30 April 2016

Keywords:
External intensity standard
Solvent subtraction
Decanoate ion
β-Cyclodextrin
Trimethyl-β-cyclodextrin
Micelles

ABSTRACT

A method for calibrating Raman intensities of diluted aqueous solutions, based on the integrated intensity of the OH stretching bands of liquid water as an external intensity standard, is described and used to obtain a difference spectrum that reveals intensity changes mainly due to the intermolecular interaction between two solutes. The method is applied to trimethyl-β-cyclodextrin in sodium decanoate aqueous solutions. The difference between the interaction spectra above and below the critical micellar concentration of sodium decanoate, in the CH stretching region between 2700 and 3100 cm^{-1}, shows an intensity increase of the CH stretching bands for trimethyl-β-cyclodextrin above the critical micellar concentration of sodium decanoate, whereas β-cyclodextrin is relatively insensitive to the presence of decanoate ion micelles in aqueous solution.

1. Introduction

Cyclodextrins (CDs), doughnut-shaped cyclic oligomers formed by (α-1,4)-linked α-D-glucopyranose units, are well known for their ability to include apolar molecules or apolar molecular fragments that fit in their cavities [1–3]. Inclusion complexation by natural CDs involves guest-host interactions that depend on several factors like the CD ring size and guest size, van der Waals interactions, release of water molecules, hydrogen-bond formation and hydrophobic interactions [4].

Methylation changes the physical and chemical properties of CDs. In particular, methylated CDs have negative solubility coefficients in water, that is, they are well soluble in cold water and slightly soluble in hot water where they usually precipitate or crystallize [5,6]. At 25 °C, the solubility of trimethyl-β-cyclodextrin (TRIMEB; 31 g/100 mL) is ca. 17 times the solubility of βCD (1.85 g/100 mL) [7]. In addition, the inclusion properties of methylated CDs are generally improved over those of natural CDs, as the complexes of methylated CDs in solution are more stable than those of natural species [4]. Due to steric hindrance involving methyl groups and the lack of intramolecular hydrogen bonds, trimethyl-CD macrocycles become distorted and their potential to discriminate chiral molecules increases as the complex formation induces conformational changes of the host molecule to suitably accommodate the guest within the CD cavity [8–13].

It has been shown by small-angle neutron scattering (SANS) that ammonium decanoate in D_2O solution originates spherical micelles [14,15]. Analysis of ^1H NMR chemical shift variations of the methyl protons of sodium decanoate in D_2O solutions leads to a critical micellar concentration (CMC) approximately equal to 116 mM and points to a narrow distribution of sizes about the mean aggregation number for decanoate ion micelles [16]. When a cyclodextrin is added to a 200 mM perdeuterated sodium decanoate NaDec(d_{19}) solution in D_2O (CMC ≈ 116 mM), methylated cyclodextrins show correlation peaks in the SANS $I(Q)$ distributions that reflect the degree of methylation, whereas αCD and βCD do not originate any correlation maximum [17], a result which seems to exclude the formation of mixed micelles, at least for this surfactant with the above mentioned concentration [18,19].

In this work, the integrated intensity of the complex of Raman OH stretching bands of liquid water is used as an external intensity standard to normalize the spectra of two solutes (trimethyl-β-cyclodextrin and sodium decanoate) aqueous solutions, and subtract the water spectrum. The resulting normalized spectra are then used to obtain difference spectra that show the interaction between both solutes, above and below sodium decanoate CMC.

* Corresponding author.
E-mail address: teixeiradias@ua.pt (J.J.C. Teixeira Dias).

http://dx.doi.org/10.1016/j.vibspec.2016.04.010
0924-2031/

2. Materials and methods

2.1. Materials and samples

Sodium decanoate (NaDec, Sigma, 98%), β-cyclodextrin (βCD, Sigma, 97%) and heptakis(2,3,6-tri-O-methyl)-β-cyclodextrin (TRIMEB, Cyclolab, 98%) were used as received without further purification. Milli-Q water was used in the preparation of all solutions and mixtures. All glassware was carefully washed with ethanol and dried before use. Five ml volumes of 60 mM and 200 mM sodium decanoate solutions were prepared by slow addition of appropriate amounts of sodium decanoate to Milli-Q water, with constant stirring. Each of these solutions was divided in two equal volumes and appropriate amounts of cyclodextrin (βCD or TRIMEB) were added to each of them to obtain solutions 30 mM in the cyclodextrin. Thus, the following aqueous solutions were obtained: 60 mM and 200 mM in sodium decanoate (D60 and D200), 30 mM in the cyclodextrin (βCD or TRIMEB) and 60 mM in sodium decanoate (B30D60 and T30D60), 30 mM in the cyclodextrin and 200 mM in sodium decanoate (B30D200 and T30D200). While the solubility of βCD at room temperature in water is 1.85 g/100 mL [7], that is, ca. 16.3 mM, its solubility in excess of sodium decanoate is far greater due to the formation of the inclusion complex, thus making possible to prepare the above sodium decanoate aqueous solutions 30 mM in βCD, at room temperature.

2.2. Raman spectrometer and dedicated software

Raman spectra were obtained at room temperature (20–21 °C), with a T64000 triple stage spectrometer in the double subtractive plus spectrograph configuration (focal distance 0.640 m, aperture f/7.5, holographic gratings of 1800 grooves mm^{-1}). A 90° geometry between the incident radiation and the collecting system was employed. The entrance slit was set to 200 μm and the intermediate slit between premonochromator and spectrograph was set to 30 mm. The detection system was a liquid nitrogen cooled non-intensified 1024 × 256 pixel (1″) charge coupled device chip. The 514.5 nm line of an Ar^+ laser (Coherent, model Innova 300-05) was used as excitation radiation, providing ca. 15 mW at the sample position. The samples were sealed in Kimax capillary tubes of 0.8 mm inner diameter. The spectra were collected with an acquisition time of 60 s for 10 accumulations. Under the above conditions, the error in the determination of frequencies is estimated to be 1 cm^{-1}.

The Raman spectrometer control and data processing were performed using the LabSpec 5.0 (Horiba, France) software. Among other utilities, this software allows to carry out baseline corrections to the spectra, apply a scaling factor to the band intensities of a spectrum, add and subtract data. All spectra were recorded from 300 cm^{-1} to 3800 cm^{-1} and a polynomial baseline correction of degree 6 was applied.

In the absence of a dedicated software for processing the Raman spectroscopic data, the interested reader can easily perform all the data processing considered in this paper by using Excel®, provided the recorded spectra can be expressed as a table with two columns, one for the Raman shifts, the other for the corresponding intensities.

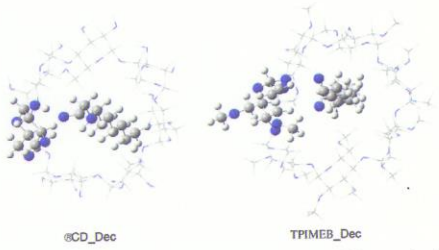

βCD_Dec TPIMEB_Dec

Fig. 1. Optimized geometries for the 1:1 inclusion complexes of decanoate ion in βCD and in TRIMEB obtained with the *Gaussian* 09 ONIOM method for two layers (B3LYP/6-31+G(d,p): UFF method).

Table 1
Calculated (scaled) frequencies (cm^{-1}) of peak intensities, in the CH stretching region, for the 1:1 inclusion complex of decanoate ion in βCD (Glu = glucose unit; s = symmetric, as = antisymmetric), and observed Raman shifts for the B30D200 spectrum.

Glu_Dec	approx. description	observed Raman shifts/cm^{-1}
2854	(Glu) CH	2856
		2875
2889, 2907	(Dec) CH_2 s	2902
2918	(Glu) CH_2 s + (Dec) CH_3 s	2920
2934	(Dec) CH_2 as	2939
2951	(Glu) CH + (Dec) CH_2 as	
2982	(Dec) CH_3 as	2970
2996	(Glu) CH_2 as	2999
3005	(Glu) CH	

2.3. Frequency calculations

Frequency and Raman intensity calculations were performed by the system of programs *Gaussian* 09 [20], with the B3LYP DFT method and the 6-31+G(d,p) basis set, the frequencies being scaled by the factor 0.964 ± 0.023 [21]. Optimized geometries for the inclusion of decanoate ion in βCD and in TRIMEB were treated with the ONIOM method for two layers, the high layer being composed by the decanoate ion and one glucosidic unit of the cyclodextrin and treated at the B3LYP/6-31+G(d,p) level, the low level being taken at the Molecular Mechanics UFF method. In the absence of inter-glucose hydrogen bonds, TRIMEB shows a somewhat distorted macrocycle (Fig. 1). Tables 1 and 2 present the calculated (scaled) frequencies (cm^{-1}) of peak intensities in the CH stretching region, their approximate descriptions and the observed frequencies.

2.4. Decomposition of the observed Raman spectra in Lorentzian-Gaussian functions

Raman spectra between 2700 cm^{-1} and 3100 cm^{-1} were decomposed using *Mathematica* [22] as the linear combination $aL + (1-a)G$, where L and G stand for Lorentzian and Gaussian functions and a represents the fraction of Lorentzian character ($1-a$ is the fraction of Gaussian character). In this fitting, the variable parameters were peak positions, peak intensities, bandwidths (FWHH) and the a parameters. Peak positions were

Table 2
Calculated (scaled) frequencies (cm^{-1}) of peak intensities, in the CH stretching region, for the 1:1 inclusion complex of decanoate ion in TRIMEB (Tmg = trimethylglucose unit; s = symmetric, as = antisymmetric), and observed Raman shifts for the T30D200 spectrum.

Tmg_Dec	approx. description	observed Raman shifts/cm^{-1}
2857	(Tmg) CH_3 s	2857
2882, 2889	(Tmg) CH_2 s, (Dec) CH_2 s	2889
2902	(Tmg) CH_3 + (Dec) CH_2 s	
2917, 2927	(Dec) CH_2 s	2931
2935, 2948	(Dec) CH_2 as	2943
2953, 3053	(Tmg) CH	
2982	(Dec) CH_3 as	
3009, 3013	(Tmg) CH_3 as	3008

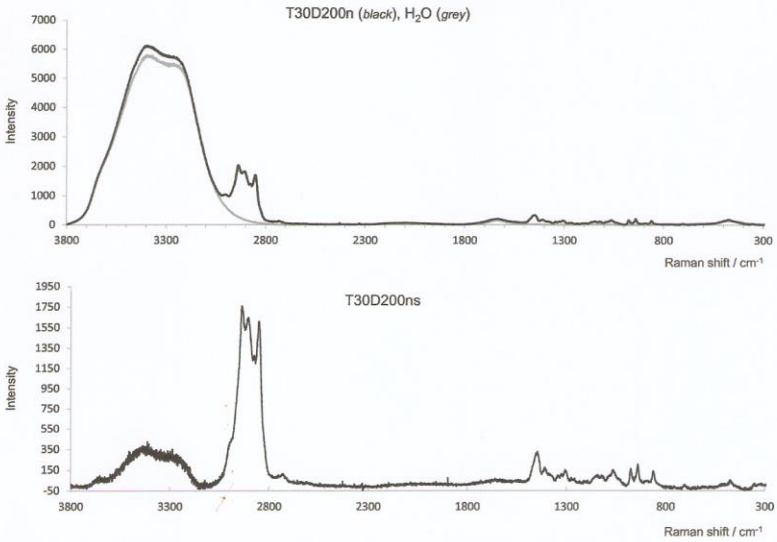

Fig. 2. Normalization of the Raman spectrum of the aqueous solution T30D200 with the Raman OH stretching bands of Milli-Q water and the Raman spectrum resulting from the subsequent subtraction of the Raman spectrum of Milli-Q water (T30D200 ns).

initially set by trial and error, followed by the fitting of bandwidths and peak intensities. The *a* parameters were fitted at last.

3. Results and discussion

3.1. The Raman OH stretching band of water as an external intensity standard

The Raman spectrum of liquid water has been the subject of a number of previous studies [23–27]. In particular, the feature between 300 cm^{-1} and 1000 cm^{-1} with maximum at ca. 470 cm^{-1} is composed by three active intermolecular librational modes [23]. In turn, the HOH bending feature, whose maximum occurs nominally at 1640 cm^{-1}, has a slightly asymmetric band shape [23]. At last, the bands between 2700 cm^{-1} and 3800 cm^{-1} are assigned to the OH stretching modes [25–27].

In diluted aqueous solutions, at ambient temperature, water concentration is approximately equal to 55.5 mol dm^{-3}, as the densities of diluted aqueous solutions do not appreciably depart from the density of pure water approximately given by 1.00 g cm^{-3} [28]. Therefore, the solvent concentration greatly exceeds the solute concentration and the Raman bands of water that correspond to group frequencies (the HOH bending and the OH stretching bands) can in principle be used as external standards to normalize the spectrum of a diluted aqueous solution. In particular, the HOH bending band is exclusively associated with the water

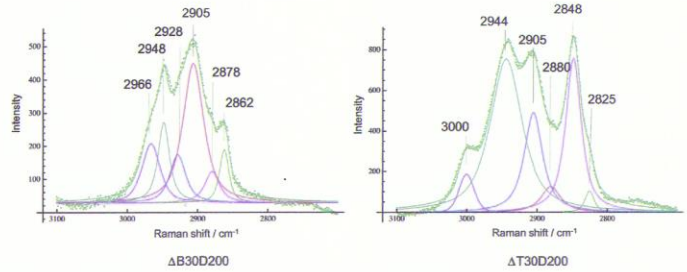

Fig. 3. Decomposition in Lorentzian-Gaussian band profiles of the ΔB30D200 and ΔT30D200 Raman spectra in the Raman CH stretching wavenumber region.

solvent. However, this is a very weak, broad and asymmetric band, sometimes lacking a well defined baseline due to interference with nearby Raman and fluorescence bands. Hence, its use as an external intensity standard can lead to appreciable errors. In turn, the OH stretching bands of liquid water are very strong and can be used in principle as an external intensity standard for normalization of Raman spectra of diluted aqueous solutions. The use as an external rather than internal intensity standard allows subtracting the water spectrum, thus obtaining the CH stretching region free from the interference with the nearby wing of the OH stretching bands, and allows obtaining difference spectra to reveal the interaction between two solutes. The OH stretching bands of water have been previously used as internal standard in a number of studies ([29–31]) to determine the concentration of various chemical species in aqueous solutions. In addition, several methods for calibrating Raman intensities have been described [32] and a comprehensive review of photometric standards for Raman spectroscopy can be found in [33].

3.2. Equilibrium concentrations

The aqueous solutions B30D60, B30D200, T30D60 and T30D200 have the cyclodextrin and decanoate ion in dynamic equilibrium with the inclusion complex. Conservation of the total cyclodextrin and decanoate concentrations is expressed by the following relationships

$$[CD]_t = [CD] + [CD_D]$$
$$[D]_t = [D] + [CD_D] \quad (1)$$

where

$$[CD_D] = K[D][CD] \quad (2)$$

and K represents the binding inclusion constant, [D] stands for the decanoate concentration in solution and in the micelles (there are equilibria involving these concentrations) and [CD_D] represents the concentration of the 1:1 inclusion complex. For B30D60 and T30D60, $[CD]_t = 30$ mM and $[D]_t = 60$ mM, whereas for B30D200 and T30D200, $[CD]_t = 30$ mM and $[D]_t = 200$ mM.

For the decanoate ion inclusion in βCD, the following binding constants have been reported: 3.7×10^3, by affinity capillary electrophoresis [34], $2.6(\pm 0.2) \times 10^3$, by spectral displacement method [35], and $7.5(\pm 0.9) \times 10^3$, by potenciometry [36]. Any of these K values yields $[\beta CD\_D] \approx 30$ mM, as there is an excess of decanoate over cyclodextrin, $[\beta CD] \approx 0$, $[D] \approx 30$ mM for B30D60 and $[D] \approx 170$ mM for B30D200. For the decanoate ion inclusion in TRIMEB, a binding constant value could not be found in the literature. However, using trial K values equal to 10^i ($i = 1–4$), the concentration values are approximately the same as those found for the βCD aqueous solutions, that is, $[TRIMEB\_D] \approx 30$ mM, $[TRIMEB] \approx 0$, $[D] \approx 30$ mM for T30D60 and $[D] \approx 170$ mM for T30D200. Since the cyclodextrin and sodium decanoate aqueous solutions, B30D60, B30D200, T30D60 and T30D200, have an excess of sodium decanoate over the corresponding cyclodextrin, the free cyclodextrin concentrations in solution are negligible.

3.3. Raman spectra for 1:1 inclusion complexes

In order to obtain the Raman spectrum due to the 1:1 inclusion complex, we need to deal with spectra that share a common intensity

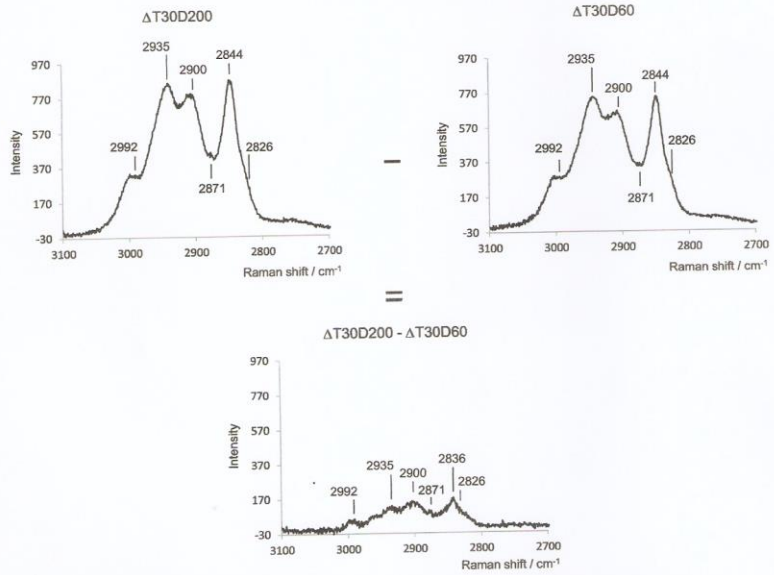

Fig. 4. The Raman spectra ΔT30D200, ΔT30D60 and their difference ΔT30D200 – ΔT30D60 in the CH stretching region.

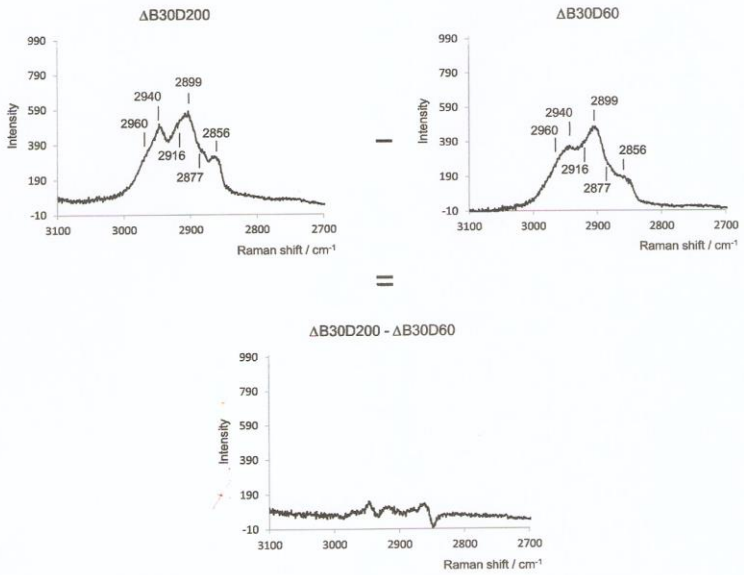

Fig. 5. The Raman spectra ΔB30D200, ΔB30D60 and their difference ΔB30D200 – ΔB30D60 in the CH stretching region.

scale. To this end, a spectrum is said to be normalized when the profile of its OH stretching bands matches as closely as possible the corresponding bands of Milli-Q water. Being impossible to obtain a perfect match in all Raman shifts, preference is given to the match on the lower wavenumber wing of this complex of bands, so that CH stretching bands become free from overlapping with the wing of the OH stretching bands. After spectral normalization, we can proceed to subtract the water spectrum.

Fig. 2 illustrates the normalization of the T30D200 spectrum and displays the spectrum resulting from water subtraction, which is named T30D200 ns, where "n" and "s" stand for normalization and subtraction of the water solvent. As an order of magnitude of the error involved in the spectral normalization, the integrated intensity of the residual OH stretching bands in the T30D200 ns spectrum amounts to 4.0% of the integrated intensity of the complex of the OH stretching bands of Milli-Q water.

In order to subtract the spectrum corresponding to the excess of decanoate ion present in the T30D200 aqueous solution and obtain the interaction spectrum for the 1:1 inclusion complex ΔT30D200, we take the following spectral difference ΔT30D200 = T30D200 ns – (170/200)D200 ns, as [TRIMEB_D] ≈ 30 mM, [TRIMEB] ≈ 0 and [D] ≈ 170 mM.

Fig. 3 shows the decomposition of the ΔB30D200 and ΔT30D200 spectra in linear combinations of Lorentzian and Gaussian functions. For ΔB30D200, this analysis reveals bands with peak intensities at 2862 cm^{-1}, 2878 cm^{-1}, 2905 cm^{-1}, 2928 cm^{-1}, 2948 cm^{-1} and 2966 cm^{-1}, while the decomposition of the ΔT30D200 spectrum exhibits peak intensities at 2825 cm^{-1}, 2848 cm^{-1}, 2880 cm^{-1}, 2905 cm^{-1}, 2944 cm^{-1} and 3000 cm^{-1}.

Fig. 4 shows the ΔT30D200, ΔT30D60 and ΔT30D200-ΔT30D60 Raman spectra (difference between the 1:1 inclusion complex spectra, above and below the decanoate ion CMC), in the CH stretching region between 2700 cm^{-1} and 3100 cm^{-1}. In turn, Fig. 5 comprises the spectra for the βCD aqueous solutions, namely, ΔB30D200, ΔB30D60 and ΔB30D200-ΔB30D60. While the ΔT30D200-ΔT30D60 spectrum indicates a significant intensity increase above the sodium decanoate CMC, with respect to the corresponding intensities below the sodium decanoate CMC (Fig. 4), the ΔB30D200-ΔB30D60 spectrum shows less significant positive and negative intensity variations (Fig. 5). The different behaviours of TRIMEB and βCD in their interaction with sodium decanoate micelles come in line with the previously reported SANS results, where it was found that methylated cyclodextrins show correlation peaks in the $I(Q)$ distributions, whereas αCD and βCD do not originate any correlation maximum [17].

4. Conclusions

Raman spectra of diluted aqueous solutions are usually dominated by the very intense complex of OH stretching bands of the water solvent. An aqueous solution containing two weakly interacting solutes A and B yields a spectrum where it may be difficult to identify frequency and intensity variations due to the AB complex of weakly interacting solute molecules. Based on the integrated intensity of the complex of OH stretching bands of liquid water as an external intensity standard, this paper showed how to obtain a difference spectrum that reveals Raman intensity changes mainly due to the intermolecular interaction between the interacting solutes, provided one knows the equilibrium concentrations of A, B and AB species in aqueous solution. In addition, this method allows to qualitatively distinguish the behaviour of TRIMEB and βCD in an aqueous solution of sodium decanoate

above and below its CMC, in accordance with previously published data on these systems [17].

Acknowledgement

The authors thank financial support from the Portuguese Foundation for Science and Technology—UID/MULTI/00070/2013.

References

[1] J. Szejtli, Chem. Rev. 98 (1998) 1743–1754.
[2] W. Saenger, J. Jacob, K. Gessler, T. Steiner, D. Hoffmann, H. Sanbe, K. Koizumi, S. M. Smith, T. Takaha, Chem. Rev. 98 (1998) 1787–1802.
[3] K. Harata, Chem. Rev. 98 (1998) 1803–1828.
[4] M.V. Rekharsky, Y. Inoue, Chem. Rev. 98 (1998) 1875–1918.
[5] K. Harata, Recent advances in the X-ray analysis of cyclodextrin complexes, in: J.L. Atwood, J.E.D. Davies, D.D. MacNicol (Eds.), Inclusion Compounds, Inorganic and Physical Aspects of Inclusion, vol. 5, Oxford University Press, 1991, pp. 311–344.
[6] A. Kusmin, R.E. Lechner, M. Kammel, W. Saenger, J. Phys. Chem. B 112 (2008) 12888–12898.
[7] K. Uekama, T. Irie, Pharmaceutical applications of methylated cyclodextrin derivatives, in: D. Duchene (Ed.), Cyclodextrins and Their Industrial Uses, Editions de Santé, Paris, 1987, pp. 395–439.
[8] K. Harata, K. Uekama, M. Otagiri, F. Hirayama, Bull. Chem. Soc. Jpn. 56 (1983) 1732–1736.
[9] K. Harata, F. Hirayama, T. Imai, K. Uekama, M. Otagiri, Chem. Lett. 6 (1984) 443–460.
[10] K. Harata, K. Uekama, M. Otagiri, F. Hirayama, Bull. Chem. Soc. Jpn. 60 (1987) 497–502.
[11] K. Harata, K. Uekama, T. Imai, F. Hirayama, M. Otagiri, J. Incl. Phenom. 6 (1988) 443–460.
[12] V. Crupi, G. Guella, D. Majolino, I. Mancini, A. Paciaroni, B. Rossi, V. Venuti, P. Verrocchio, G. Viliani, Philos. Mag. 91 (2011) 1776–1785.
[13] V. Crupi, G. Guella, D. Majolino, I. Mancini, B. Rossi, R. Stancanelli, V. Venuti, P. Verrocchio, G. Viliani, Food Biophys. 6 (2011) 267–273.
[14] S.J. Burkitt, R.H. Ottewill, J.B. Hayter, B.T. Ingram, Colloid Polym. Sci. 265 (1987) 619–627.
[15] R.M. Clapperton, R.H. Ottewill, A.R. Rennie, B.T. Ingram, Colloid Polym. Sci. 277 (1999) 15–24.
[16] C. Andrade-Dias, S. Lima, J.J.C. Teixeira-Dias, J. Colloid Interface Sci. 316 (2007) 31–36.
[17] S. Andrade-Dias, J.J.C. Teixeira-Dias, J. Teixeira, J. Phys. Chem. B 112 (2008) 15327–15332.
[18] Y. Kusumoto, M. Shizuka, Chem. Phys. Lett. 125 (1986) 64–68.
[19] R. Guo, X.J. Zhu, X. Guo, Colloid Polym. Sci. 281 (2003) 876–881.
[20] M.J. Frisch, G.W. Trucks, H.B. Schlegel, G.E. Scuseria, M.A. Robb, J.R. Cheeseman, G. Scalmani, V. Barone, B. Mennucci, G.A. Petersson, H. Nakatsuji, M. Caricato, X. Li, H.P. Hratchian, A.F. Izmaylov, J. Bloino, G. Zheng, J.L. Sonnenberg, M. Hada, M. Ehara, K. Toyota, R. Fukuda, J. Hasegawa, M. Ishida, T. Nakajima, Y. Honda, O. Kitao, H. Nakai, T. Vreven, J.A. Montgomery Jr., J.E. Peralta, F. Ogliaro, M. Bearpark, J.J. Heyd, E. Brothers, K.N. Kudin, V.N. Staroverov, R. Kobayashi, J. Normand, K. Raghavachari, A. Rendell, J.C. Burant, S.S. Iyengar, J. Tomasi, M. Cossi, N. Rega, J.M. Millam, M. Klene, J.E. Knox, J.B. Cross, V. Bakken, C. Adamo, J. Jaramillo, R. Gomperts, R.E. Stratmann, O. Yazyev, A.J. Austin, R. Cammi, C. Pomelli, J.W. Ochterski, R.L. Martin, K. Morokuma, V.G. Zakrzewski, G.A. Voth, P. Salvador, J.J. Dannenberg, S. Dapprich, A.D. Daniels, Ö. Farkas, J.B. Foresman, J.V. Ortiz, J. Cioslowski, D.J. Fox, Gaussian 09, Revision A.1, Gaussian, Inc., Wallingford, CT, 2009.
[21] **NIST Computational Chemistry Comparison and Benchmark Database, NIST Standard Reference Database Number 101, in: Russell D. Johnson III (Ed.), NIST Computational Chemistry Comparison and Benchmark Database, 2015. Release 17b, September, 2015** http://cccbdb.nist.gov/.
[22] Mathematica®, Version 10.2.0.0, Platform Mac OS X, Wolfram Research Inc., Champaign, Illinois, 2010.
[23] D.M. Carey, G.M. Korenowski, J. Chem. Phys. 108 (1998) 2669–2675.
[24] M.R. Walrafen, M.S. Fisher, J. Chem. Phys. 85 (1986) 6970–6982.
[25] Q. Wan, L. Spanu, G.A. Galli, F. Gygi, J. Chem. Theory Comput. 9 (2013) 4124–4130.
[26] Z. Wang, A. Pakoulev, Y. Pang, D.D. Dlott, J. Phys. Chem. 108 (2004) 9054–9063.
[27] Q. Sun, Vib. Spectrosc. 51 (2009) 213–217.
[28] Handbook of Chemistry and Physics on CD-ROM, Version 2011, in: W.M. Haynes (Ed.), CRC Press, Taylor and Francis Group, 2011.
[29] Q. Sun, C. Qin, Chem. Geol. 283 (2011) 274–278.
[30] T. Azbej, M.J. Severs, B.G. Rusk, R.J. Bodnar, Chem. Geol. 237 (2007) 255–263.
[31] J. Wu, H.F. Zheng, Chem. Geol. 273 (2010) 267–271.
[32] R.N. Favors, Y. Jiang, Y.L. Loethen, D. Ben-Amotz, Rev. Sci. Instrum. 76 (2005) 033108.
[33] R.L. McCreery, Photometric standards for Raman spectroscopy, in: J.M. Chalmers, P.R. Griffiths (Eds.), Handbook of Vibrational Spectroscopy, John Wiley & Sons Ltd., Chichester, 2002.
[34] K.M. Parker, A.M. Stalcup, J. Chromatogr. A 1204 (2008) 171–182.
[35] M.M. Meier, M.T.B. Luiz, P.J. Farmer, B. Szpoganicz, J. Incl. Phenom. Mol. Recognit. Chem. 40 (2001) 291–295.
[36] R.I. Gelb, L.M. Schwartz, J. Incl. Phenom. Mol. Recognit. Chem. 7 (1989) 465–476.

APPENDIX

A
P
P
E
N
D
I
X
1

H_2O spectrum

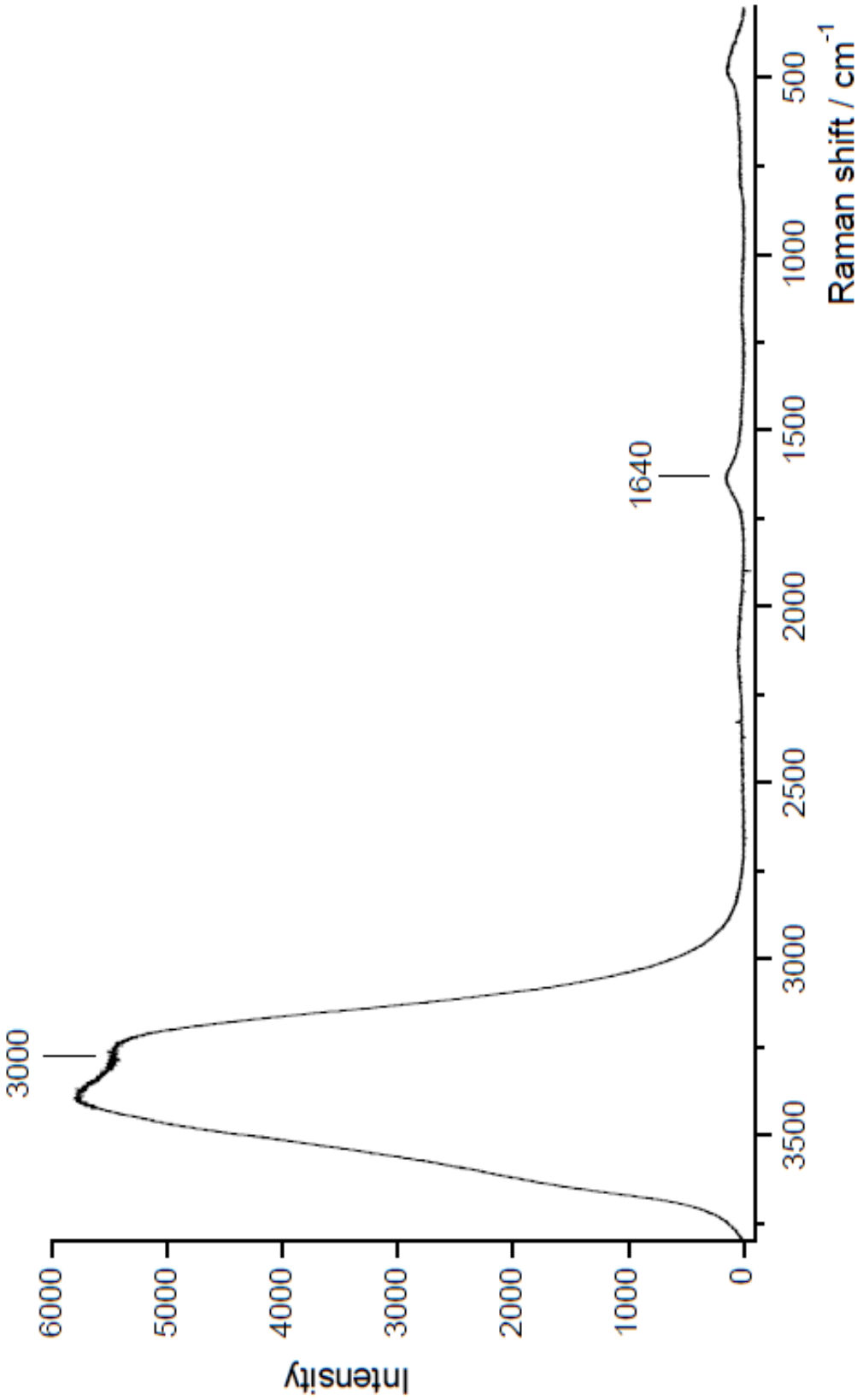
Intensity
6000
5000
4000
3000
2000
1000
0
3000
1640
3500
3000
2500
2000
1500
1000
500
Raman shift / cm-1

A
P
P
E
N
D
I
X
2

Normalization and subtraction of water spectrum

T30D60ns

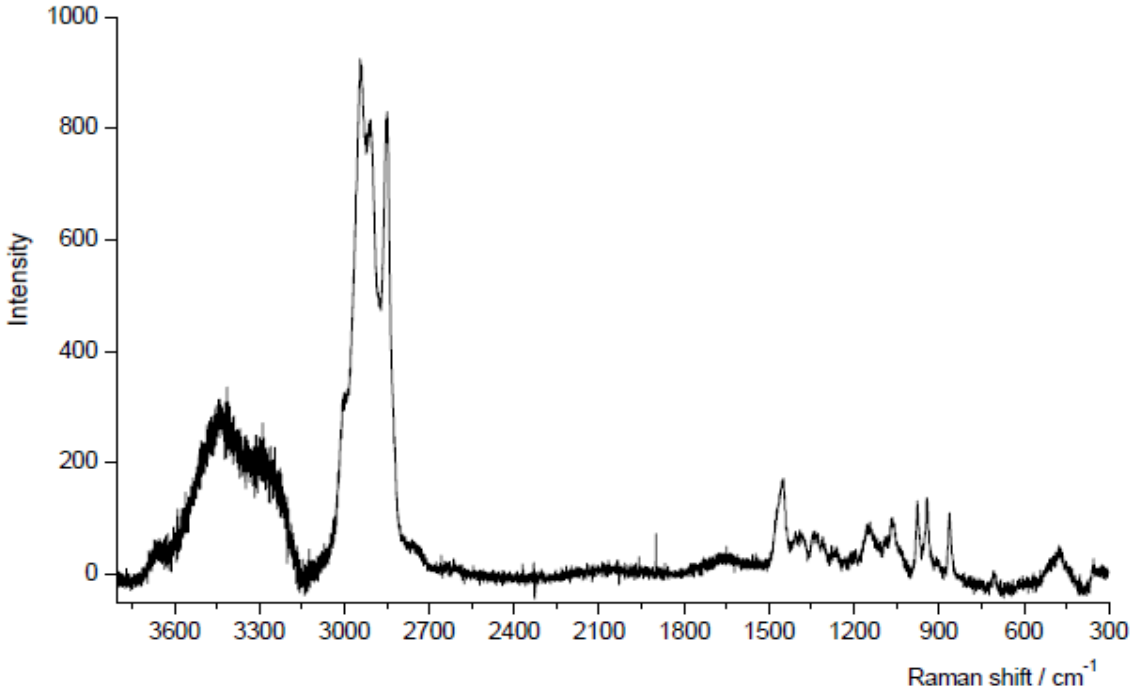

B30D200ns

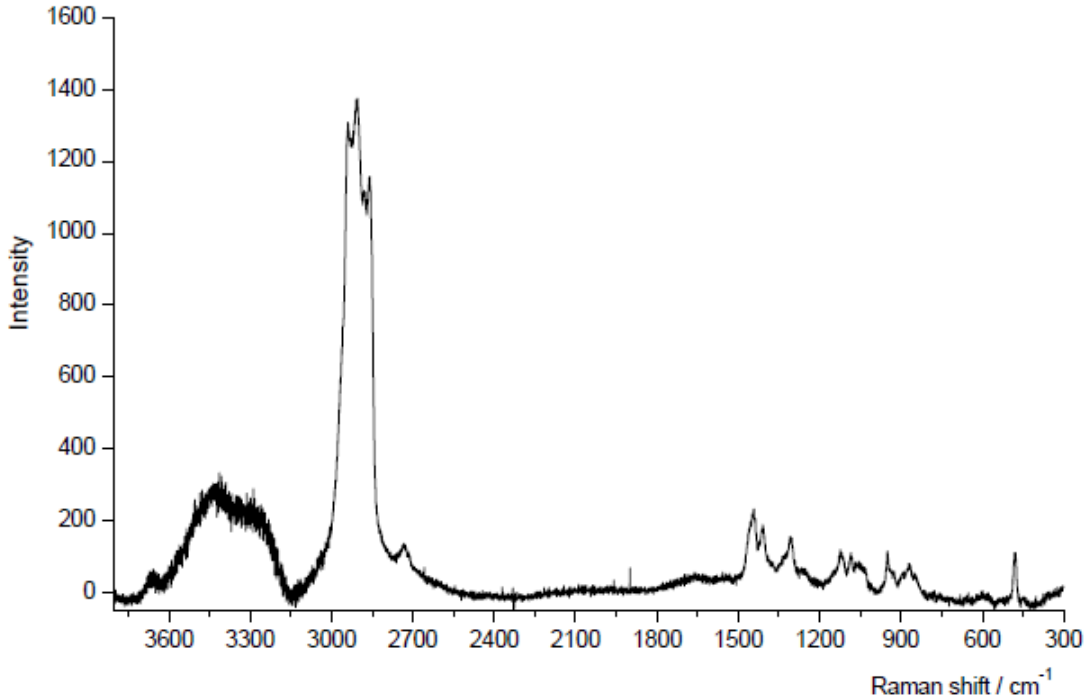

B30D60ns

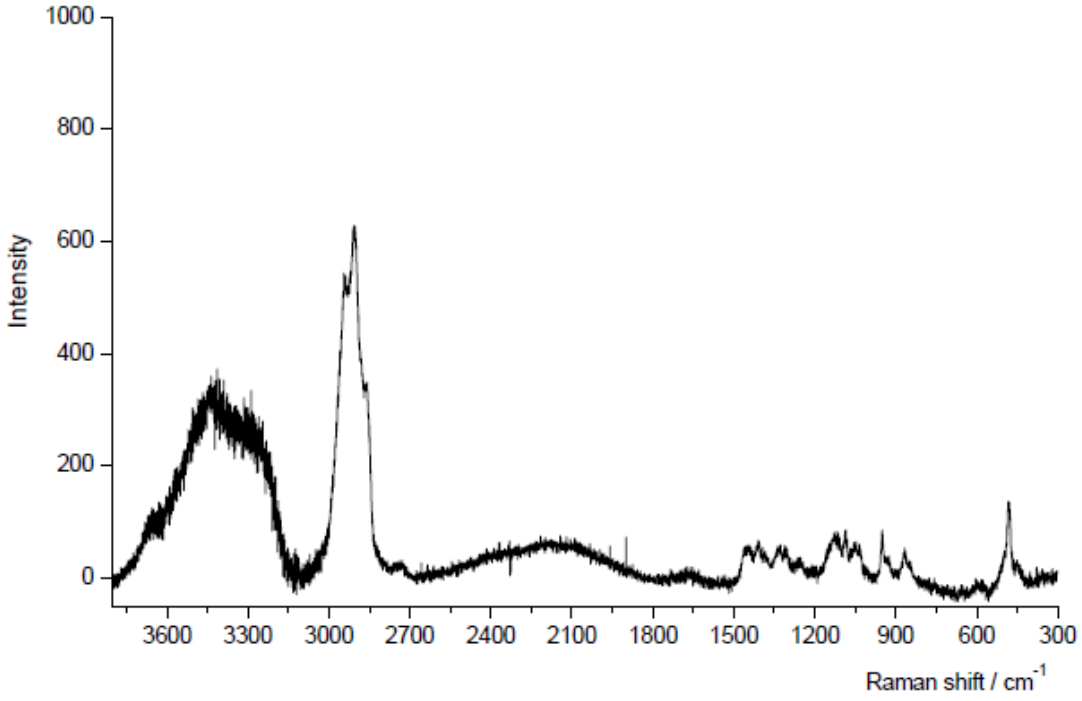

D200ns

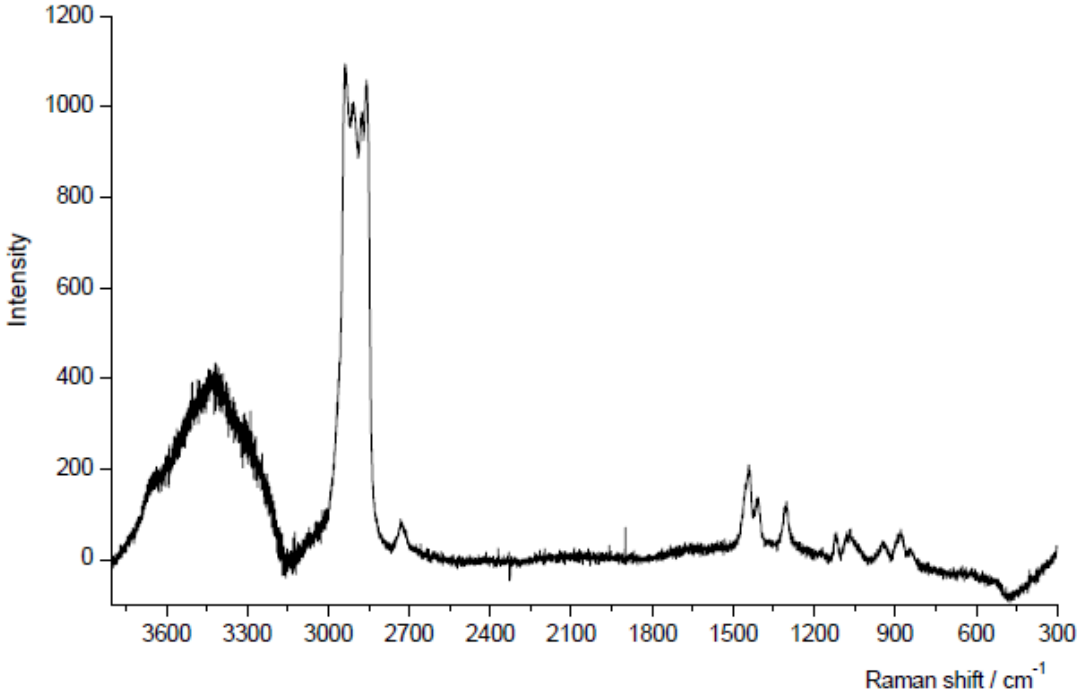

D60ns

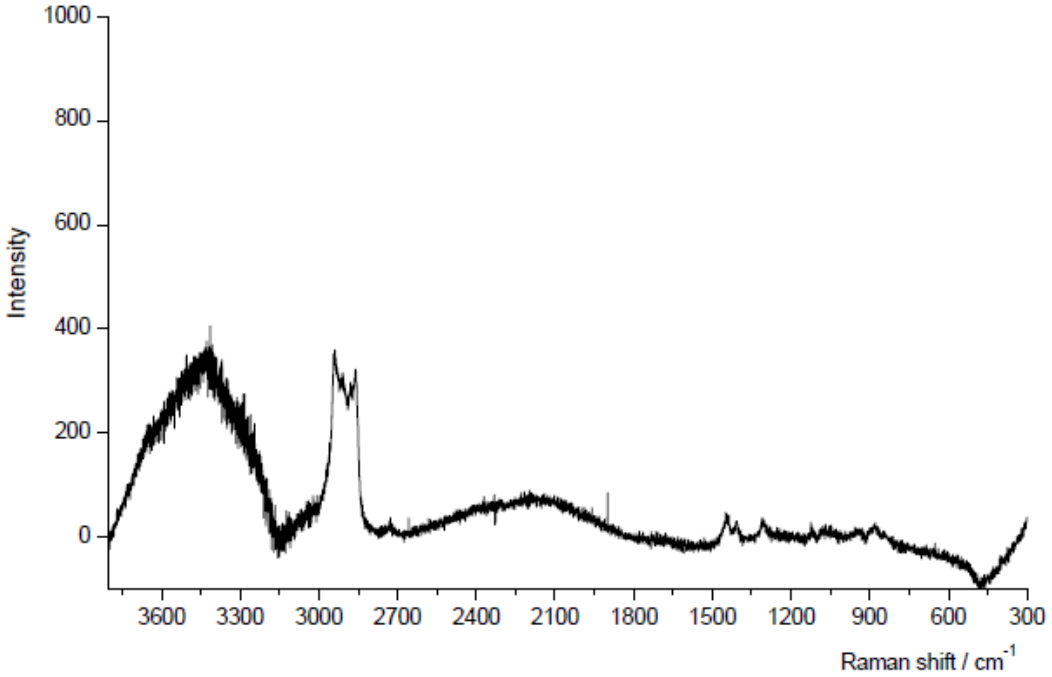
1000
800
600
400
200
0
Intensity
3600
3300
3000
2700
2400
2100
1800
1500
1200
900
600
300
Raman shift / cm-1

A
P
P
E
N
D
I
X
3

\

Methylate cyclodextrin in aqueous solution

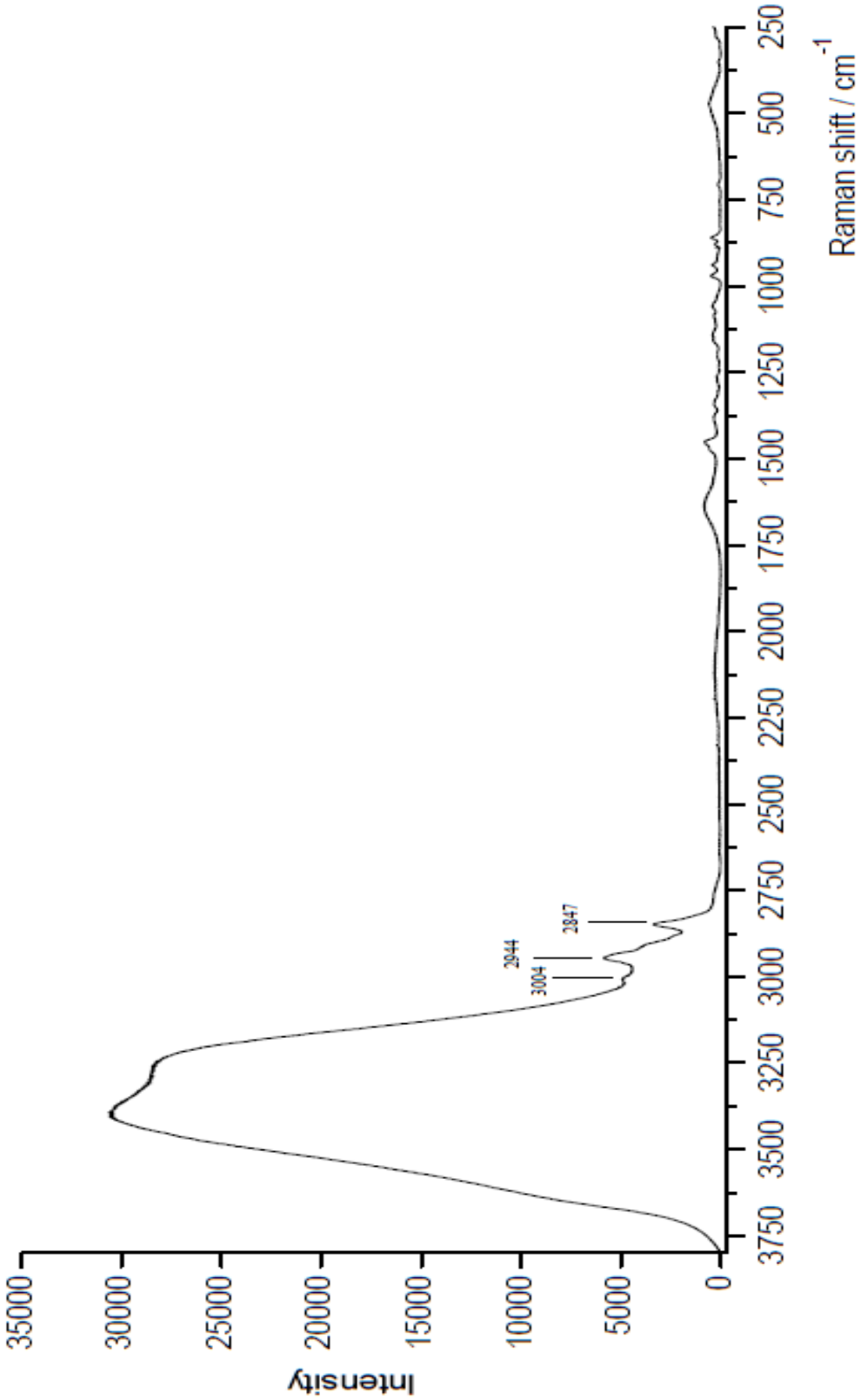
Intensity
35000
30000
25000
20000
15000
10000
5000
0
3750
3500
3250
3000
2750
2500
2250
2000
1750
1500
1250
1000
750
500
250
Raman shift / cm-1
2944
3004
2847